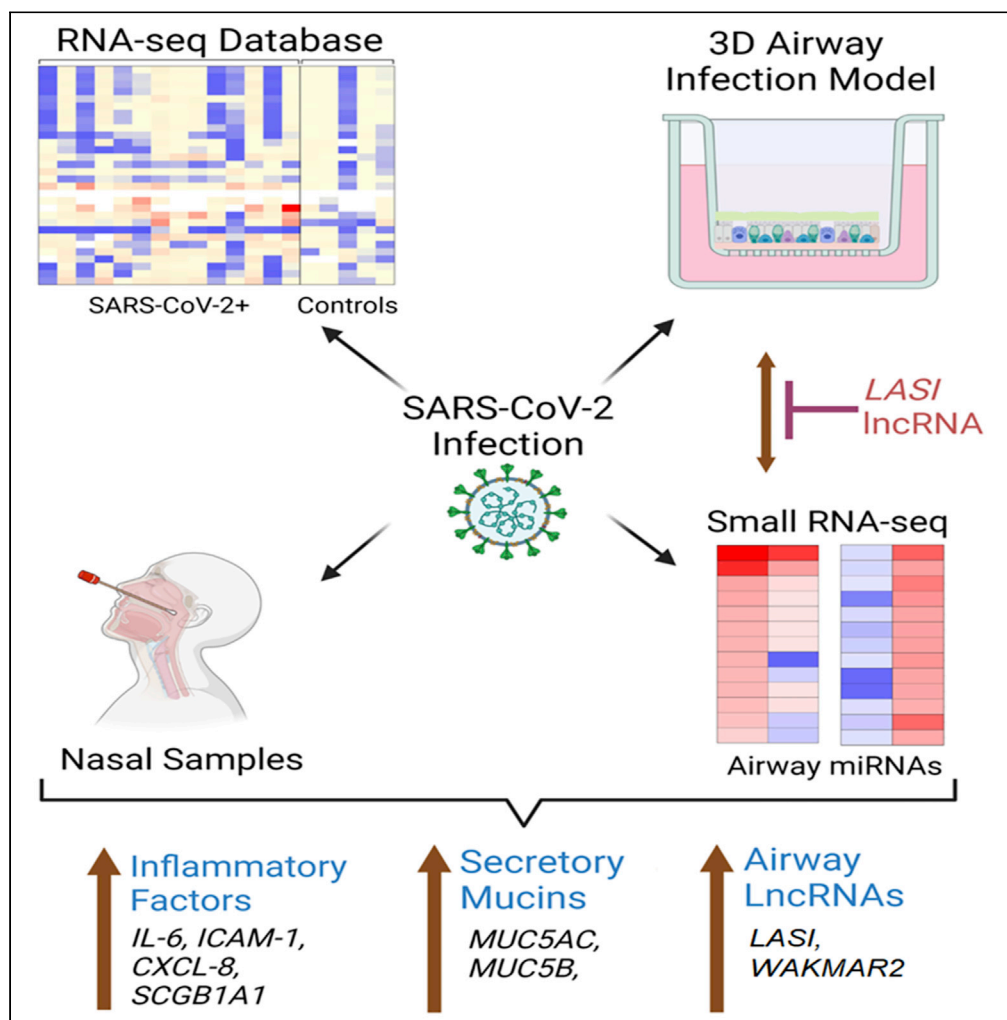CellPress
OPEN ACCESS

Article

Immunomodulatory LncRNA on antisense strand of ICAM-1 augments SARS-CoV-2 infection-associated airway mucoinflammatory phenotype

Dinesh Devadoss,
Arpan Acharya,
Marko Manevski,
..., Glen M.
Borchert,
Siddappa N.
Byrareddy,
Hitendra S. Chand

sid.byrareddy@unmc.edu
(S.N.B.)
hchand@fiu.edu (H.S.C.)

Highlights

COVID19 airway
mucoinflammatory
response strongly
correlates with *LASI*
lncRNA level

Silencing *LASI* lncRNA
suppresses SARS-CoV-2
viral load and associated
inflammation

LASI lncRNA shows a
potential direct
interaction with SARS-
CoV-2 spike viral RNA

Hosts of airway epithelial
miRNAs are modulated by
LASI to regulate
inflammation

iScience

Article

Immunomodulatory LncRNA on antisense strand of ICAM-1 augments SARS-CoV-2 infection-associated airway mucoinflammatory phenotype

Dinesh Devadoss,[1] Arpan Acharya,[2] Marko Manevski,[1] Dominika Houserova,[3] Michael D. Cioffi,[4] Kabita Pandey,[2] Madhavan Nair,[1] Prem Chapagain,[4,5] Mehdi Mirsaeidi,[6,7] Glen M. Borchert,[3] Siddappa N. Byrareddy,[2,*] and Hitendra S. Chand[1,8,*]

SUMMARY

Noncoding RNAs are important regulators of mucoinflammatory response, but little is known about the contribution of airway long noncoding RNAs (lncRNAs) in COVID-19. RNA-seq analysis showed a more than 4-fold increased expression of *IL-6*, *ICAM-1*, *CXCL-8*, and *SCGB1A1* inflammatory factors; *MUC5AC* and *MUC5B* mucins; and *SPDEF*, *FOXA3*, and *FOXJ1* transcription factors in COVID-19 patient nasal samples compared with uninfected controls. A lncRNA on antisense strand to ICAM-1 or *LASI* was induced 2-fold in COVID-19 patients, and its expression was directly correlated with viral loads. A SARS-CoV-2-infected 3D-airway model largely recapitulated these clinical findings. RNA microscopy and molecular modeling indicated a possible interaction between viral RNA and *LASI* lncRNA. Notably, blocking *LASI* lncRNA reduced the SARS-CoV-2 replication and suppressed MUC5AC mucin levels and associated inflammation, and select *LASI*-dependent miRNAs (e.g., let-7b-5p and miR-200a-5p) were implicated. Thus, *LASI* lncRNA represents an essential facilitator of SARS-CoV-2 infection and associated airway mucoinflammatory response.

INTRODUCTION

Vaccination efforts have significantly reduced the spread of COVID-19, although variants arising from genomic mutations pose a significant risk even among vaccinated people (Fageeh et al., 2021; Kannan et al., 2022; Vitale et al., 2021). SARS-CoV-2 gains entry via the upper respiratory mucosa, and any host factor dysregulations occurring during this interaction can result in pulmonary and/or extrapulmonary complications (Hoffmann et al., 2020; Hou et al., 2020; Olwenyi et al., 2020; Rothan and Byrareddy, 2020). In the first week of infection, viral shedding and replication are relatively predominant in upper respiratory tract (Ravindra et al., 2021). During these events, virus evades host's mucosal and innate immune responses, allowing it to move toward the lower respiratory tract and eventually to systemic invasion (He et al., 2020). As such, limiting shedding and viral replication in the upper respiratory tract blocks disease progression, and various immunomodulators regulate the expression of viral receptors and entry factors. That said, besides being the protective barrier and a competent airway lumen clearance mechanism, airway mucins typically moderate the mucosal immune responses (Hewitt and Lloyd, 2021). During SARS-CoV-2 infection, however, induced inflammatory factors drive airway tissue remodeling, and severe inflammation can cause mucus hyperexpression potentially leading to acute respiratory distress syndrome (ARDS).

Analyzing host-viral interactions is vital for understanding viral pathogenesis. Several notable protein interactions necessary for SARS-CoV-2 infection and/or progression are now well documented; specific roles for the host lncRNAs during SARS-CoV-2 infection remain elusive. Roles for lncRNAs in regulating virtually every cellular function have now been reported including moderating the immune response of infected host cells as well as regulating the genomic packing and replication of several viruses (Devadoss et al., 2019; Statello et al., 2021; Yao et al., 2019). LncRNAs play a vital role in regulating the innate immune responses, and recent studies have shown that specific lncRNAs are differentially expressed during host-pathogen interactions following viral infection (Blanco-Melo et al., 2020; Natarelli et al., 2021; Turjya et al., 2020; Vishnubalaji et al., 2020). Although a few reports have examined lncRNA expression profiles

[1]Department of Immunology and Nano-Medicine, Herbert Wertheim College of Medicine, Florida International University, Miami, FL 33199, USA

[2]Department of Pharmacology and Experimental Neuroscience, University of Nebraska Medical Center, Omaha, NE 68198, USA

[3]Department of Pharmacology, University of South Alabama, Mobile, AL 36688, USA

[4]Department of Physics, Florida International University, Miami, FL 33199, USA

[5]Biomolecular Sciences Institute, Florida International University, Miami, FL 33199, USA

[6]Miller School of Medicine, Division of Pulmonary, Critical Care, and Sleep Medicine, University of Miami, Miami, FL 33136, USA
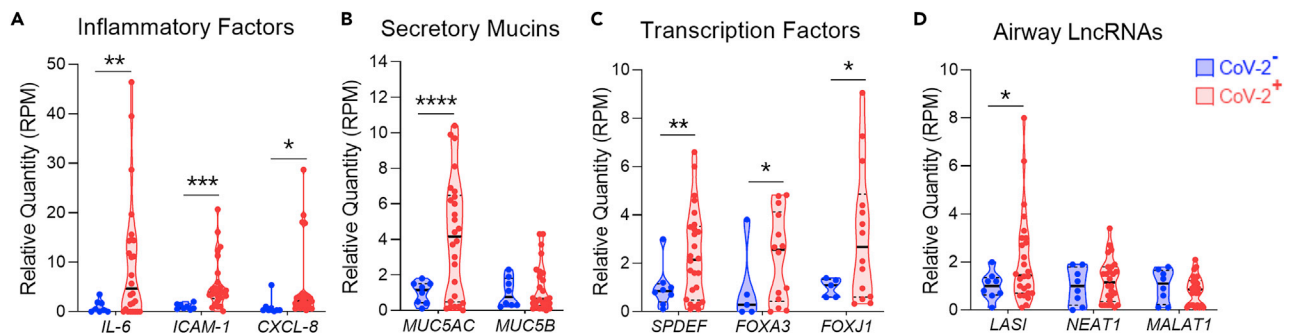
[7]Present address: Division of Pulmonary, Critical Care and Sleep, College of Medicine-Jacksonville, University of Florida, Jacksonville, FL 32218, USA

[8]Lead contact

*Correspondence:
sid.byrareddy@unmc.edu (S.N.B.),
hchand@fiu.edu (H.S.C.)

https://doi.org/10.1016/j.isci.2022.104685

Figure 1. Expression levels of transcripts encoding inflammatory factors, airway secretory mucins, associated transcription factors, and select lncRNAs in the RNA-seq database of nasopharyngeal swabs of SARS-CoV-2 positive individuals

(A–D) Relative expression of (A) airway inflammatory factors *IL-6*, *ICAM-1*, and *CXCL-8* mRNAs; (B) airway mucins *MUC5AC* and *MUC5B* mRNAs; (C) transcription factors *SPDEF*, *FOXA3*, and *FOXJ1* mRNAs; and (D) lncRNAs *LASI*, *NEAT1*, and *MALAT1* in SARS-CoV-2 positive (CoV-2$^+$) individuals compared with SARS-CoV-2 negative (CoV-2$^-$) control individuals. The expression levels were calculated from the transcript reads per million (RPM) RNA-seq data (Table S1) of nasopharyngeal swabs from CoV-2$^+$ subjects (n = 26) compared with CoV-2$^-$ control subjects (n = 8) as reported recently (Cheemarla et al., 2021). (Data shown as violin plots with individual data points, medians, and quartiles; *p < 0.05; **p < 0.01; ***p < 0.001; ****p < 0.0001 by Student's t test). Similar increased expression of *IFIH1* and *SCGB1A1* mRNAs was observed in CoV-2$^+$ subjects (Figure S1).

for stratifying the COVID-19 disease severity and associated immune dysfunction (Cheng et al., 2021; Meydan et al., 2020; Morenikeji et al., 2020; Mukherjee et al., 2021), studies examining roles of respiratory epithelial specific lncRNAs in SARS-CoV-2 infection are far more limited (Blanco-Melo et al., 2020; Vishnubalaji et al., 2020). Our recent studies identified a novel epithelial lncRNA *LASI* differentially expressed during the mucus hypersecretory response (Devadoss et al., 2021a). In this study, we have assessed the acute mucoinflammatory response, i.e., the excessive mucus expression, inflammation, other immunomodulatory factors, and lncRNAs in a 3D airway tissue model of acute SARS-CoV-2 infection and COVID-19 patient nasopharyngeal samples to gain novel insights into early innate responses of human respiratory cells.

RESULTS

SARS-CoV-2-infected individuals show induced airway mucoinflammatory responses and increased LASI lncRNA expression

The mucosal immune response of the upper respiratory tract plays a critical role in viral entry, replication and dissemination of systemic infection, and expiratory shedding. Several innate immunoregulatory transcripts of both protein-coding and noncoding RNAs are implicated in the SARS-CoV-2 infection and host antiviral response, yet very few validated roles of lncRNAs have been reported. Therefore, we performed an analysis of the airway immune response in publicly available RNA sequencing datasets obtained from SARS-CoV-2-positive (CoV-2$^+$) patients and uninfected (CoV-2$^-$) controls (Table S1, GeneSet Accession: PRJNA730941) (Cheemarla et al., 2021). Our initial analysis examined RNA-seq files obtained from nasal swab samples of 26 CoV-2$^+$ and eight CoV-2$^-$ controls. We specifically analyzed for the lung mucoinflammatory response genes and associated lncRNAs, and the expression levels of *IL-6*, *ICAM-1*, and *CXCL-8* mRNAs were around 10-, 6-, and 5-fold higher in CoV-2$^+$ individuals, respectively, compared with CoV-2$^-$ controls (Figure 1A). Among the intracellular viral RNA sensor genes analyzed, there was a 3-fold increased expression of *IFIH1* (MDA-5) mRNA in CoV-2$^+$ individuals with no significant change in *DDX58* (RIG-1) and the downstream mediator *IRF3* mRNA expression compared with healthy CoV-2$^-$ controls (Figure S1A).

Although roles for airway mucins in innate antiviral immunity are well documented (Ridley and Thornton, 2018; Weitnauer et al., 2016), SARS-CoV-2-infection-associated mucin signatures have not been thoroughly evaluated to date (Lu et al., 2021). Notably, the airway secretory mucin *MUC5AC* mRNA levels in the present cohort were 4-fold higher in CoV-2$^+$ individuals than in CoV-2$^-$ controls (Figure 1B), and there was no significant change in *MUC5B* mRNA levels. The mRNA levels for mucin transcriptional regulators (Chen et al., 2014; Rajavelu et al., 2015), *SPDEF* and *FOXA3*, as well as the ciliogenesis transcriptional factor, *FOXJ1*, were 2- to 3-fold higher among CoV-2$^+$ individuals (Figure 1C). There was no change in *FOXA2* and *FOXM1* transcription factors (Figure S1B) but the mRNA levels of airway secretoglobulin *SCGB1A1* was 3-fold lower among CoV-2$^+$ individuals (Figure S1B). The expression levels of host factors facilitating the viral entry, such as *ACE2*, *NRP1*, *DPP4*, *IFITM*, and *DDX1* as well as the Spike protein processing cellular

Table 1. Demographics of COVID-19 patients whose nasopharyngeal swab samples were analyzed

|	Lo-VL	Hi-VL	p-value
Subjects	10 (7)	10 (5)	—
Sex (M/F)	6M/4F	7M/3F	—
Age (Y)	61.5 ± 4.0	63.1 ± 3.8	0.8163
SARS-CoV-2 N1 vRNA (C_T)	35.5 ± 0.7	25.9 ± 1.3	<0.0001
Hospitalization	7	5	—
Hypertension	5	5	—
Diabetes	4	0	—
Infectious Disease	1	2	—
Pneumonia	5	5	—
Oxygen Supplementation (>6L O_2)	1	5	—
ICU	3	5	—
ARDS	3	5	—
Obesity	5	3	—

Medical history was available for twelve patients.

proteases such as *TMRPSS2*, *Furin*, *CTSB*, *CTSL*, and *TMPRSS11D* showed no significant change between CoV-2 positive versus negative individuals (data not shown).

We have recently characterized airway lncRNAs that play essential roles in innate immune responses of respiratory mucosa (Devadoss et al., 2019, 2021a) and propose that these immunomodulatory lncRNAs may be dysregulated during SARS-CoV-2 infection and thus drive the COVID-19-associated respiratory comorbidities. Among the immunomodulatory lncRNAs analyzed (Figure 1D), we found a lncRNA antisense to intercellular adhesion molecule 1 (ICAM-1) or *LASI*, described recently (Devadoss et al., 2021a), showed 2-fold higher expression in CoV-2$^+$ individuals compared with CoV-2$^-$ controls. In contrast, expression levels of *NEAT1* or nuclear enriched abundant transcript-1 (Li et al., 2020; Maltezou et al., 2021; Vishnubalaji et al., 2020) and *MALAT1* or metastasis associated lung adenocarcinoma transcript-1 (Cui et al., 2019) lncRNAs exhibited no significant change (Figure 1D). Thus, our analyses indicate that compared with CoV-2$^-$ controls, the airway mucoinflammatory gene signature is strongly correlated with induced *LASI* lncRNA expression among CoV-2$^+$ individuals.

COVID-19-positive individuals with higher viral load show increased mucoinflammatory response

Recent epidemiological and clinical studies suggest that there is no difference in SARS-CoV-2 viral load between symptomatic and asymptomatic CoV-2$^+$ individuals; however, disease severity and mortality rate among symptomatic individuals is directly correlated with airway viral load (Fajnzylber et al., 2020; Lee et al., 2020; Maltezou et al., 2021). Therefore, to assess the correlation of viral load with mucoinflammatory responses and associated lncRNAs, we examined the nasopharyngeal swab samples procured locally from twenty CoV-2$^+$ individuals (Table 1). Viral load in each subject was determined by qRT-PCR for SARS-CoV-2 N1 nucleocapsid viral RNA (vRNA) levels and were assigned as low-viral load (Lo-VL) or high-viral load (Hi-VL) CoV-2$^+$ samples based on the cycle threshold (C_T) values of >30 or <30, respectively (Figure S2A). Applying this threshold, 10 subjects were characterized as Hi-VL (C_T = 25.9 $\pm$ 1.3; 7M/3F, 63.1 $\pm$ 3.8 years) and 10 as Lo-VL (C_T = 35.5 $\pm$ 0.7; 6M/4F, 61.5 $\pm$ 4.0 years), with Hi-VL subjects exhibiting 100-fold higher CoV-2 vRNA levels than Lo-VL subjects (Figure 2A). Interestingly, no significant differences were observed between the two groups in *ACE2* (Figure S2B) and *TMPRSS2* (Figure S2C) mRNA levels. Among antiviral interferon responsive genes, we failed to detect *DDX58*, *IFIH1*, *IRF3*, and *IFNG* transcripts, and there was no difference in *IFNB1* mRNA levels between Hi-VL and Lo-VL samples (Figure S2D). In contrast, Hi-VL samples exhibited ~1.5-fold higher *IL-6* (Figure 2B) and *ICAM-1* (Figure 2C) mRNAs compared with Lo-VL samples. The expression levels analyzed in individual samples showed that *IL-6* (Figure S3A) and *ICAM-1* (Figure S3B) mRNAs significantly correlated with CoV-2 N1 viral RNA levels, showing distinct clustering of Hi-VL and Lo-VL subjects.
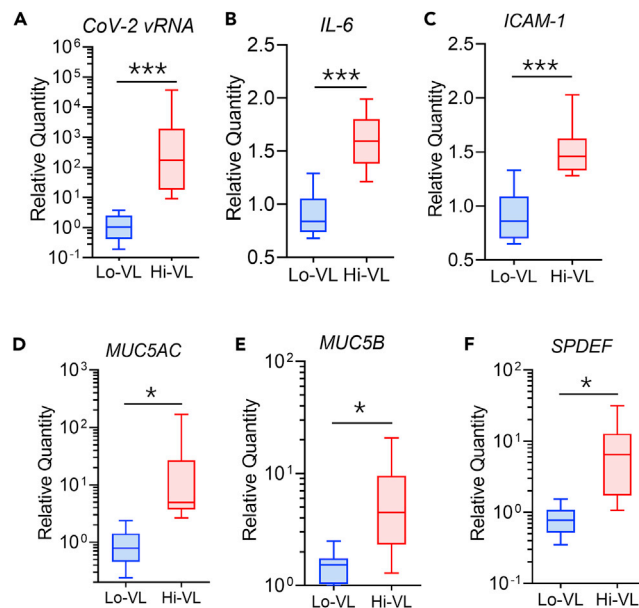
Figure 2. COVID-19 positive individuals with high nasopharyngeal viral load show increased mucoinflammatory phenotype compared with low viral load individuals

(A–F) Total RNA from nasopharyngeal swab samples of COVID-19 positive individuals (n = 20) was analyzed. Based on the SARS-CoV-2 nucleocapsid viral RNA expression, the individuals with high viral load (Hi-VL) had average C_T values of 25.9 ± 1.3 (n = 10), whereas those with low viral load (Lo-VL) had average C_T values of 35.5 ± 0.7 (n = 10). Relative mRNA expression of (A) SARS-CoV-2 viral RNA (CoV-2 vRNA); innate inflammatory factors, (B) IL-6, and (C) ICAM-1; airway mucins (D) MUC5AC and (E) MUC5B; and (F) mucin regulatory transcriptional factor SPDEF in Hi-VL compared with Lo-VL patient swab samples. (Data shown as box and whisker plots with minimum to maximum range; n = 10/gp; *p < 0.05; **p < 0.01; ***p < 0.001 by Student's t test). Increased expression of MUC4 and SCGB1A1 mRNAs was also observed in Hi-VL subjects with no changes in select viral entry facilitating host factor mRNAs and IFN1B mRNA expression (Figure S2) and select host mucoinflammatory genes and lncRNAs strongly correlated with CoV-2 viral load (Figure S3).

In agreement with RNA-seq database analyses (Figure 1), all of the nasal swab samples in our study cohort showed upregulated mucin expression with Hi-VL samples exhibiting robust ∼10-fold higher MUC5AC (Figure 2D) and 4-fold higher MUC5B (Figure 2E) mucin mRNA levels. Notably, although Hi-VL subjects trended toward lower MUC2 mRNA expression (Figure S2E), they exhibited ∼10-fold higher MUC4 (Figure S2F) mRNA expression. SPDEF mRNA expression was also increased by ∼5-fold in Hi-VL subjects (Figure 2F), and surprisingly, SCGB1A1 expression was ∼4-fold higher in Hi-VL subjects (Figure S2G). However, when analyzed individually, there was no significant correlation (p = 0.0596) between MUC5AC expression levels and CoV-2 viral RNA levels (Figure S3C), although SPDEF mRNA levels showed a strong correlation (Figure S3D). These data indicate that SARS-CoV-2 viral load dictates the extent of airway mucin and associated inflammatory factor expression among COVID-19-positive individuals.

Innate immunomodulatory lncRNAs are associated with SARS-CoV-2 viral load

Next, we analyzed the expression levels of select airway lncRNAs in our cohort. We found that compared with the Lo-VL samples, the expression levels of lncRNA LASI (Figure 3A), NEAT1 (Figure 3B), and a wound and keratinocyte-migration-associated lncRNA 2 (WAKMAR2) (Figure 3D) were all significantly upregulated in Hi-VL samples, whereas lncRNA MALAT1 levels were not altered (Figure 3C). When analyzed individually, the expression levels of lncRNA LASI (Figure S3E), NEAT1 (Figure S3F), and WAKMAR2 (Figure S3G) significantly correlated with CoV-2 viral RNA levels, with lncRNA LASI showing the highest correlation ($r^2 = 0.6381$; p < 0.0001). These data suggest that LASI lncRNA, which plays pivotal role in airway innate responses (Devadoss et al., 2021a), may be involved in SARS-CoV-2-associated airway inflammation.

Next, we performed an RNA-FISH analysis to examine LASI lncRNA expression in airway epithelial cells of nasal swab samples and cells labeled for SARS-CoV-2 N1 vRNA. Compared with Lo-VL samples, SARS-CoV-2 N1 vRNA and LASI transcripts were enriched in perinuclear and cytosolic regions with increased expression of LASI in Hi-VL subjects (Figure 3E). In agreement with qRT-PCR analyses (Figure 3A), the H-score
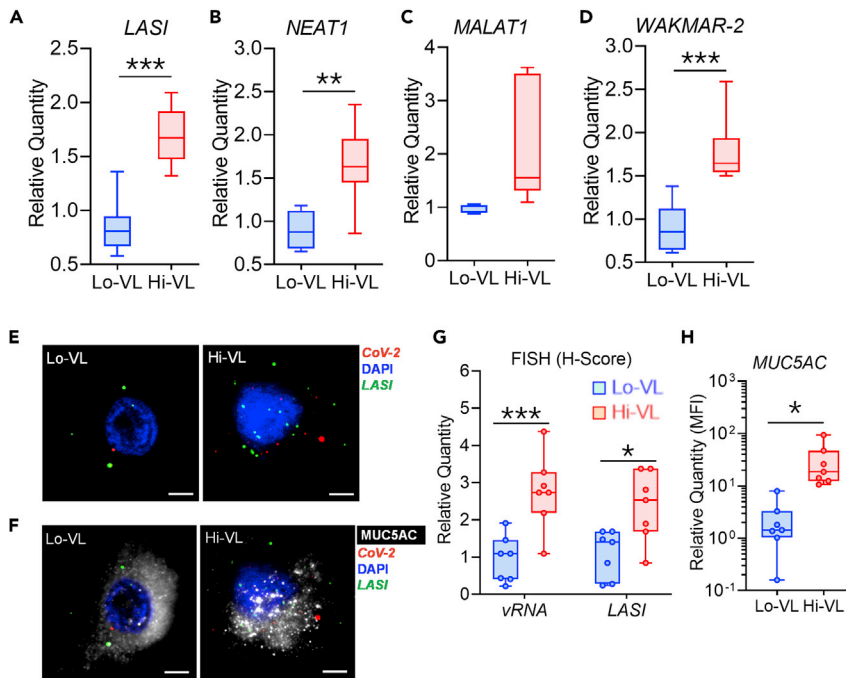
Figure 3. COVID-19 positive individuals with high viral load show increased immunomodulatory lncRNAs and the secretory mucin MUC5AC expression

(A–D) Relative expression of immunomodulatory lncRNAs, (A) *LASI*, (B) *NEAT1*, (C) *MALAT1*, and (D) *WAKMAR2* in Hi-VL compared with Lo-VL individuals' swab samples.

(E) The dual-FISH analysis detected colocalization of SARS-CoV-2 viral RNA (vRNA) and *LASI* lncRNA in nasal swab samples. Representative micrographs from Lo-VL and Hi-VL swab samples display detection of SARS-CoV-2 nucleocapsid (CoV-2) vRNA (green) and *LASI* lncRNA (red) along with DAPI-stained nuclei (blue).

(F) Nasal swab cells showing immunoreactive MUC5AC expression (shown in white) in the dual-FISH labeled cells; scale bar: 2 μm.

(G) H-score quantitation of *vRNA* and *LASI* lncRNA in COVID-19-positive individuals.

(H) Relative quantitation of mean fluorescence intensity (MFI) of MUC5AC expression in Lo-VL and Hi-VL swab samples. (n = 10/gp for data in A, B, C, & D; and n = 7/gp for data in G & H with 10 cells analyzed per sample; *p < 0.05; **p < 0.01; ***p < 0.001 by Student's t test). There was no change in MUC5B expression levels in Lo-VL and Hi-VL samples (Figure S4).

values that denote RNA expression per cell, as described recently (Devadoss et al., 2021a), were 2.7- and 2.4-fold higher for *vRNA* and *LASI* lncRNA, respectively, in Hi-VL compared with Lo-VL samples (Figure 3G). The protein expression of MUC5AC mucin as determined by immunopositivity was ~16-fold higher in Hi-VL versus Lo-VL samples (Figures 3F and 3H) with no noticeable change in MUC5B expression (Figures S4A and S4B). These datasets indicate that the immunomodulatory *LASI* lncRNA expression is significantly induced in Hi-VL than Lo-VL patient cells, and its expression strongly correlates with MUC5AC mucin expression in airway cells corroborating the RNA-seq data (Figure 1).

3D airway tissue model of SARS-CoV-2 infection demonstrates an immediate-early hyper-mucoinflammatory response

To better understand the association of CoV-2-induced airway inflammatory response and *LASI* lncRNA, a 3D airway tissue culture model of SARS-COV-2 infection was employed. Briefly, the primary human airway epithelial cells differentiated on air-liquid interface to mimic the conducting airway epithelium were infected with one MOI of SARS-CoV-2 primary clinical isolate (USA-WI1/2020). CoV-2 vRNA load was followed in apical washes, in the basal culture supernatant, and in cells at 0, 1, 4, 24, and 48 h postinfection (hpi). In apical washes, 0.89×10^5 viral genomic equivalents per mL were observed at 1 hpi, increasing to 20.2, 31.2, and 14.7×10^5 at 4, 24, and 48 hpi, respectively (Figure 4A). Viral load in basal media supernatant was 0.3×10^5 per mL at 1 hpi then increased to 3.6, 4.3, and 5.0×10^5 at 4, 24, and 48 hpi, respectively (Figure S5A). The cellular level of CoV-2 vRNA increased by 2.0-, 7.0-, and 2.6-fold at 4, 24, and 48 hpi, respectively, compared with 1 hpi (Figure 4B). Thus, 3D airway cells were productively infected with
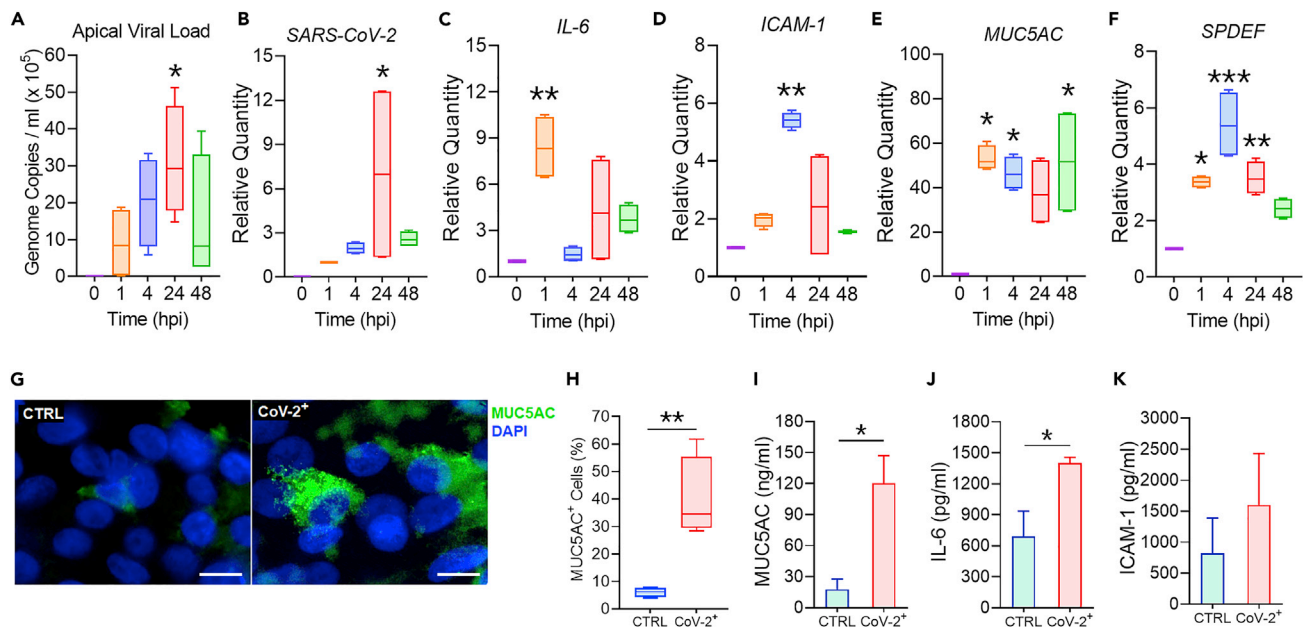
Figure 4. SARS-CoV-2 infection of human respiratory epithelial cells induces robust mucoinflammatory response in a 3D airway tissue model

(A–F) Respiratory airway epithelial cells differentiated on air-liquid interface were infected with one MOI of SARS-CoV-2 clinical isolate (USA-WA1/2020 isolate) and analyzed at 0, 1, 4, 24, and 48 h postinfection (hpi). Viral loads were determined in (A) the apical washes and (B) the total cellular RNA. Relative expression levels of the inflammatory factors, (C) *IL-6*, and (D) *ICAM-1* mRNA; and (E) airway mucin *MUC5AC*; and (F) *SPDEF* transcriptional factor in the total cellular RNA was analyzed by qRT-PCR. (n = 4/gp; *p < 0.05; **p < 0.01; ***p < 0.001 by ANOVA).

(G) Representative micrographs of uninfected control (CTRL) and SARS-CoV-2-infected (CoV-2+) cells showing MUC5AC (shown in green) immunoreactivity along with the DAPI stained nuclei (shown in blue); scale bar: 5 μm.

(H) Percentage of MUC5AC+ cells within each treatment group.

(I–K) Secreted protein levels of (I) MUC5AC mucin in apical washes and (J) IL-6 and (K) ICAM-1 in culture media supernatants as determined by specific ELISA assays (n = 4/gp; *p < 0.05; **p < 0.01; by Student's t test). There was a significant suppression of viral entry host factors with elevated expression of other mucin genes and *SCGB1A1* mRNA following CoV-2 infection (Figure S5).

SARS-CoV-2 clinical isolate, and the virions were shed at ∼ 10-fold higher levels from the apical surface than the basal region.

The expression of *ACE2* mRNA was more than 3-fold suppressed in infected at all time-points analyzed (Figures S5B), and *TMPRSS2* mRNA levels showed no change at 1, 4, and 24 hpi but was significantly reduced at 48 hpi (Figures S5C). Thus, SARS-CoV-2 infection modulates *ACE2* and *TMRPSS2* expression, as reported earlier (Fliesser et al., 2021; Matusiak and Schurch, 2020). Expression of *IL-6* mRNA was 8.0-fold induced at 1 hpi with no change at 4, 24, and 48 hpi, although there was a trend toward induced expression (Figure 4C). *ICAM-1* mRNA expression was 2.0-, 5.4-, and 2.4-fold higher at 1, 4, and 24 hpi, respectively, with no change at 48 hpi (Figure 4D). Expression of neither *NRP1* (data not shown) nor *CXCL-8* (Figure S5D) mRNA was affected following infection. However, the expression of *SCGB1A1* was induced by 4- to 5-fold at 1, 4, and 24 hpi (Figure S5E).

Interestingly, SARS-CoV-2 infection robustly upregulated *MUC5AC* mRNA expression by 53-, 46-, 37-, and 51-fold at 1, 4, 24, and 48 hpi, respectively (Figure 4E). *MUC5B* mRNA levels was also highly upregulated following infection by 13-, 11-, 16-, and 33-fold at 1, 4, 24, and 48 hpi, respectively (Figure S5F). Similarly, *MUC2* mRNA levels were 8-, 9-, 10-, and 13-fold at 1, 4, 24, and 48 hpi, respectively (Figure S5G), whereas *MUC4* mRNA levels were induced by 5-fold at 24 hpi (Figure S5H). In addition, there was a 3- to 5-fold induction in *SPDEF* mRNA levels (Figure 4F) and more than a 25-fold induction in *FOXA3* mRNA levels following CoV-2 infection (Figure S5I).

MUC5AC protein expression was assessed by immunofluorescence and quantified by ELISA to corroborate these results. In agreement with qRT-PCR analyses, CoV-2-infected (CoV-2+) cells showed robust MUC5AC immunopositivity (Figure 4G) with as much as ∼40% MUC5AC+ cells observed at 48 hpi compared with

6.0% in uninfected (CoV-2⁻) controls (Figure 4H). In addition, apical wash MUC5AC protein levels were ~10-fold higher in CoV-2+ cells with ~120 ng/mL compared with 18 ng/mL observed in uninfected cells (Figure 4I). The secreted interleukin-6 (IL-6) levels were at 691 pg/mL in uninfected cells compared with 1400 pg/mL in the CoV-2$^+$ cells at 48 hpi (Figure 4J), and ICAM-1 protein levels showed a trend toward increased expression from 823 pg/mL in uninfected cells to 1600 pg/mL in CoV-2$^+$ cells (Figure 4K). Remarkably, there was no change in the expression of *DDX58*, *IFIH1*, *IRF3*, and *IFNB1* in CoV-2 infected cells at 0, 1, and 48 hpi (Figure S6A–S6D).

SARS-CoV-2 infection induces LASI lncRNA expression that could potentially interact with CoV-2 spike viral RNA

In agreement with the increased *LASI* lncRNA observed in COVID-19 individuals, there was induced expression of *LASI* lncRNA at 0, 1, 4, 24, and 48 hpi in our 3D model of CoV-2 infection (Figure 5A). Dual-RNA FISH analyses showed CoV-2 *N1 vRNA* and *LASI* transcripts co-expression around the nuclear/perinuclear region (Figure 5B) with nearly 2-fold more lncRNAs in CoV-2+ cells as assessed by H-score analysis (Figures 5C and 5D). We also analyzed the expression of other lncRNAs, and in contrast to recent reports (Li et al., 2020; Maltezou et al., 2021; Vishnubalaji et al., 2020), the expression of lncRNA *NEAT1* (Figure S6E) and *MALAT1* (Figure S6F) was significantly reduced in CoV-2-infected cells at 0, 1, and 48 hpi, whereas *WAKMAR2* lncRNA levels were induced by more than 7-fold at 48 hpi (Figure S6G).

As FISH analyses strongly suggest *LASI* lncRNA and SARS-CoV-2 vRNA may colocalize, the potential for direct interaction was assessed informatically. Notably, our sequence analyses identified a single, high-scoring potential base-pairing between SARS-CoV-2 Spike vRNA (CoV-2 vRNA) and a specific *LASI* lncRNA sequence. The segment of the modeled CoV-2 vRNA (sequence 1198-1268 nts) after minimization and equilibration is shown in Figure 5E. This region forms a hairpin where 1227-1237 nts are intra-sequence base-paired with 1244–1254 nts (Figure 5F). 3D modeling predicts a structure where this CoV-2 vRNA region can duplex with *LASI* lncRNA bases 635-646 nts with a stable base-paired model obtained upon relaxing the structure for 100 ns of MD simulation (Figure 5G and see Video S1 online at supplemental data). This structure shows a partially unfolded CoV-2 vRNA sequence with excellent base-pairing with the *LASI* lncRNA sequence (Figure 5H). Compared with the intra-sequence base-pairing in CoV-2 vRNA in Figure 5F, the inter-sequence base-pairing with *LASI* lncRNA is energetically more favorable (−9.6 kcal/mol versus −15.0 kcal/mol) at the local interacting region. Moreover, this *LASI* lncRNA interacting region is conserved among CoV-2 variants of concern (VOCs) such as delta and omicron (Figure S7). Taken together, our experimental and molecular docking simulation studies suggest that *LASI* lncRNA may serve as the molecular scaffold for CoV-2 vRNA to assist in viral infection and replication.

Blocking LASI lncRNA expression attenuates CoV-2-altered antiviral interferon response effects and suppresses infection-dependent MUC5AC induction

To determine the role of *LASI* lncRNA in CoV-2 infection and associated mucoinflammatory response, we depleted *LASI* levels using RNAi (siRNA) technology. Briefly, 3D cultured cells transfected with either *LASI*-targeting siRNA (siLASI) or a control siRNA (siCTRL) were infected with one MOI of SARS-CoV-2 clinical isolate and then analyzed at 48 hpi. Compared with siCTRL-transfected cells, siLASI-transfected cells exhibited a 7-fold reduction in *LASI* lncRNA expression (Figure 6A). Surprisingly, we observed a marked >27-fold reduction in CoV-2 vRNA load in siLASI-transfected cells (Figure 6B). Furthermore, although *ICAM-1* (Figure S8A), *IL-6* (Figure S8B), *IFNB1* (Figure S8C), and *IFIH1* (Figure S8D) mRNA expressions were unaffected, mRNA levels of the antiviral interferon response gene, *IRF3*, were significantly reduced in siLASI-transfected cells (Figure 6C). In contrast, levels of *DDX58* mRNA were conversely induced compared with the siCTRL-transfected cells (Figure 6D). Among mucin genes, *MUC5AC* mRNA levels in siLASI-transfected cells showed a trend toward lower expression (Figure 6E) with no change in *MUC5B* mRNA levels (Figure S8E); however, *MUC2* (Figure S8F) and *MUC4* (Figure S8G) mRNAs were reduced following CoV-2 infection in siLASI-transfected cells compared with siCTRL-transfected cells. Notably, expressions of the *SPDEF* (Figure S8H) and the lncRNA *MALAT1* (Figure S8I) and *WAKMAR2* (Figure S8J) were not altered by siLASI treatment during CoV-2 infection.

To further explore potential effects on mucin genes, we next immunoprobed for MUC5AC protein expression in siCTRL and siLASI transfected cells infected with CoV-2 at 48 hpi (Figure 6F). We found siLASI treatment resulted in a >2-fold reduction of MUC5AC+ cells, where siCTRL-transfected cells had around 17.7% cells showing MUC5AC immunopositivity compared with 7.4% among siLASI-transfected cells (Figure 6G).
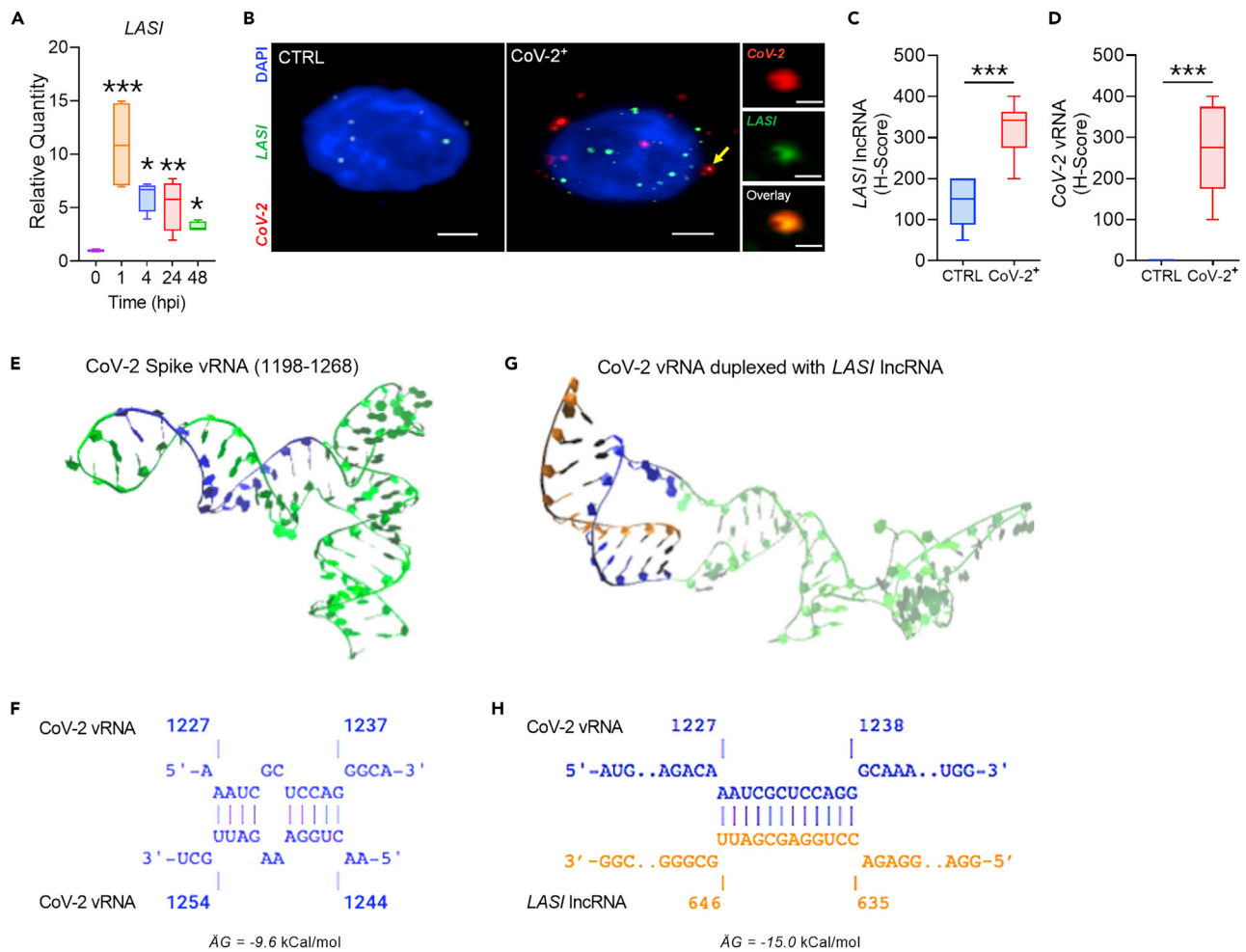
Figure 5. SARS-CoV-2 infection induces *LASI* lncRNA expression in human respiratory epithelial cells that potentially show direct interaction with CoV-2 spike RNA

(A) Relative expression levels of *LASI* lncRNA in SARS-CoV-2-infected cells at 0, 1, 4, 24, and 48 hpi. (n = 4/gp; *p < 0.05; **p < 0.01; ***p < 0.001 by ANOVA).

(B) Colocalization of SARS-CoV-2 *vRNA* and *LASI* transcripts in CoV-2-infected (CoV-2⁺) cells as determined by dual-FISH staining and the structured-illumination imaging analysis. Representative micrographs of dual-FISH-stained cells showing SARS-CoV-2 N1 *vRNA* (in red) and *LASI* lncRNAs (in green) along with DAPI-stained nuclei (in blue); scale bar: 2 μm.

(C and D) H-score quantitation of (C) CoV-2 *vRNA* and (D) *LASI* lncRNAs per cell in CoV-2+ and control cells. (n = 9–10 cells/gp; **p < 0.01; ***p < 0.001 by Student's t test).

(E) Modeled 3D structure of SARS-CoV-2 spike vRNA nucleotide sequence from 1198 to 1268, and the *LASI* lncRNA interacting region (1227-1237) is highlighted in blue.

(F) The intra-sequence base-pairing of spike nucleotides forms the hairpin stem structure.

(G) Modeled 3D structure of the CoV-2 Spike vRNA duplexed with *LASI* lncRNA sequence 646-635 (highlighted in orange) at the end of 100 ns simulation (see Video S1 at online supplemental data).

(H) Inter-sequence base-pairing of CoV-2 vRNA with *LASI* lncRNA sequence (shown in orange). There was no significant change in interferon-related gene expression; however, expression of other immunomodulatory lncRNAs were differentially regulated following CoV-2 infection (Figure S6). *LASI*-interacting sequence is conserved in Spike viral RNAs of CoV-2 Delta and Omicron variants (Figure S7).

In agreement, MUC5AC-specific ELISA of apical washes from siCTRL-transfected cells averaged 121 ng/mL of MUC5AC content, whereas siLASI-transfected cells averaged 47.5 ng/mL (Figure 6H), a more than 2-fold reduction. In contrast, we found ICAM-1 (Figure S8K) and IL-6 (Figure S8L) levels were not significantly changed in basal media supernatant following CoV-2 infection of siLASI-transfected cells as compared with siCTRL-transfected cells. Taken together, these data strongly suggest that *LASI* lncRNA represents an essential regulatory mediator in CoV-2 infection and the ensuing mucoinflammatory response of the respiratory airway epithelium.
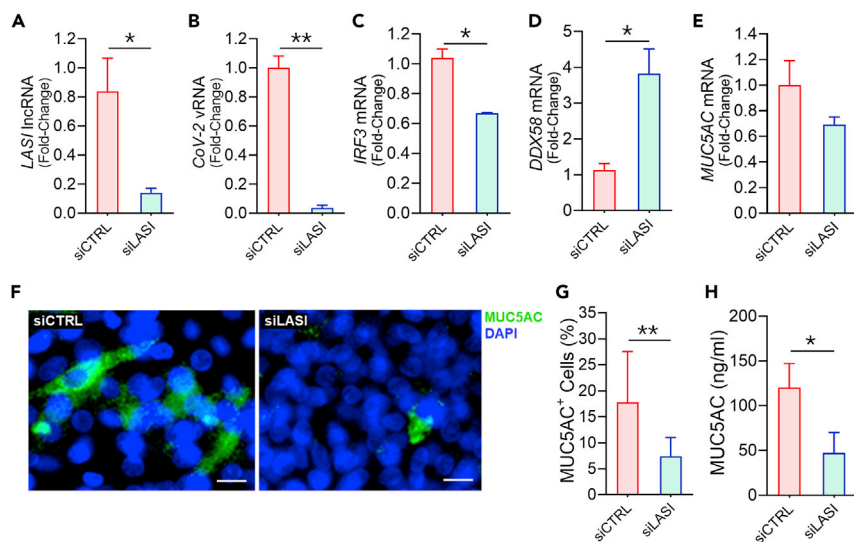
Figure 6. Blocking *LASI* lncRNA expression reduces the SARS-CoV-2 viral load and suppresses the MUC5AC mucin expression

(A–E) Relative expression of (A) *LASI* lncRNA and (B) SARS-CoV-2 vRNA in cells transfected with siRNA targeting *LASI* (siLASI) compared with control siRNA (siCTRL)-transfected cells and infected with one MOI of SARS-CoV-2. Relative expression of (C) *IRF3*, (D) *DDX58*, and (E) *MUC5AC* mRNA following SARS-CoV-2 infection in siLASI-transfected cells compared with siCTRL cells. (n = 4/gp from two independent experiments; *p < 0.05; **p < 0.01; by Student's t test).

(F) The micrographs of SARS-CoV-2-infected cells following siCTRL and siLASI transfection show MUC5AC (green) immunoreactivity and DAPI-stained nuclei (blue), scale bar: 5 μm.

(G) Percentage of MUC5AC$^+$ cells within each treatment group (n = 10/gp; **p < 0.001 by Student's t test).

(H) MUC5AC mucin protein levels in the apical wash of CoV-2-infected cells and transfected with siLASI or siCTRL as determined by ELISA assay. (n = 4/gp from two independent experiments; *p < 0.05 by Student's t test). Expression of *MUC2* and *MUC4* mucin mRNAs were also suppressed in siLASI cells with no change in expression of IL-6, ICAM-1, and other lncRNAs (Figure S8).

LASI lncRNA differentially modulates the host miRNAs associated with SARS-CoV-2 infection

LncRNAs also act as the molecular scaffold or sponge for miRNAs. Thus, they could indirectly modulate host cellular immune responses, for example, by miRNA-mediated target mRNA-decay or by competing for the same miRNA binding region, like ceRNA (Abu-Izneid et al., 2021; Siniscalchi et al., 2021; Yousefi et al., 2020; Zhang et al., 2019). In addition, host miRNAs can also directly bind to viral RNAs and/or modify the associated cell signaling mechanisms. So, to identify the miRNAs that *LASI* lncRNA may regulate, we performed a small RNA-sequencing of our 3D ALI model and analyzed for the expression of miRNAs in SARS-CoV-2-infected cells that are siLASI transfected compared with control cells. From the total of 721 miRNAs sequenced, 155 miRNAs showed significant change. Further data mining revealed a total of 38 miRNAs differentially expressed in SARS-CoV-2 infection, of which seven miRNAs (miR-4488, let-7b-5p, miR-1301-3p, miR-181b-5p, miR-2110, miR-320b, and miR-744-5p) were expressed >2 log-fold higher, whereas twenty-one miRNAs showed lower expression than uninfected cells including miR-23a-3p, miR-30d-5p, miR-200a-5p, miR-200b-3p, and miR-1246. Interestingly, knocking down the *LASI* lncRNA reverted the expression levels of several of these miRNAs; for example, some of the miRNAs induced by CoV-2 infection were suppressed by silencing LASI lncRNA (Figure 7A), of which miR-4488, let-7b-5p, miR-584-5p, miR125-1-3p, and miR-181b-5p showed very high expression in siLASI-transfected and CoV-2-infected cells. At the same time, there were miRNAs suppressed by CoV-2 infection that were highly induced in siLASI-transfected cells, e.g., miR-151a-3p, miR-6510-3p, miR-200a-5p, miR-197-3p, and miR-4644-3p (Figure 7B). The changes in the expression levels of select miRNAs were confirmed by qPCR analysis of siCTRL and siLASI cells where levels of miR-4488 (Figure 7C), let-7b-5p (Figure 7D), miR-150-5p (Figure 7E), miR-6510-3p (Figure 7F), miR-200a-5p (Figure 7G), and miR-197-3p (Figure 7H) were confirmed to be reverted in siLASI-transfected cells compared with siCTRL-transfected cells. We also confirmed the expression levels of these lncRNA *LASI*-regulated miRNAs in nasal swab samples of our cohort and of these miRNAs (Figure S9). Expression levels of let-7b-5p, miR-150-5p, and miR-200a-5p showed a viral-load dependent increased expression. Thus, these data suggest that let-7B-5p, miR-150-5p, and miR-200a-5p may be
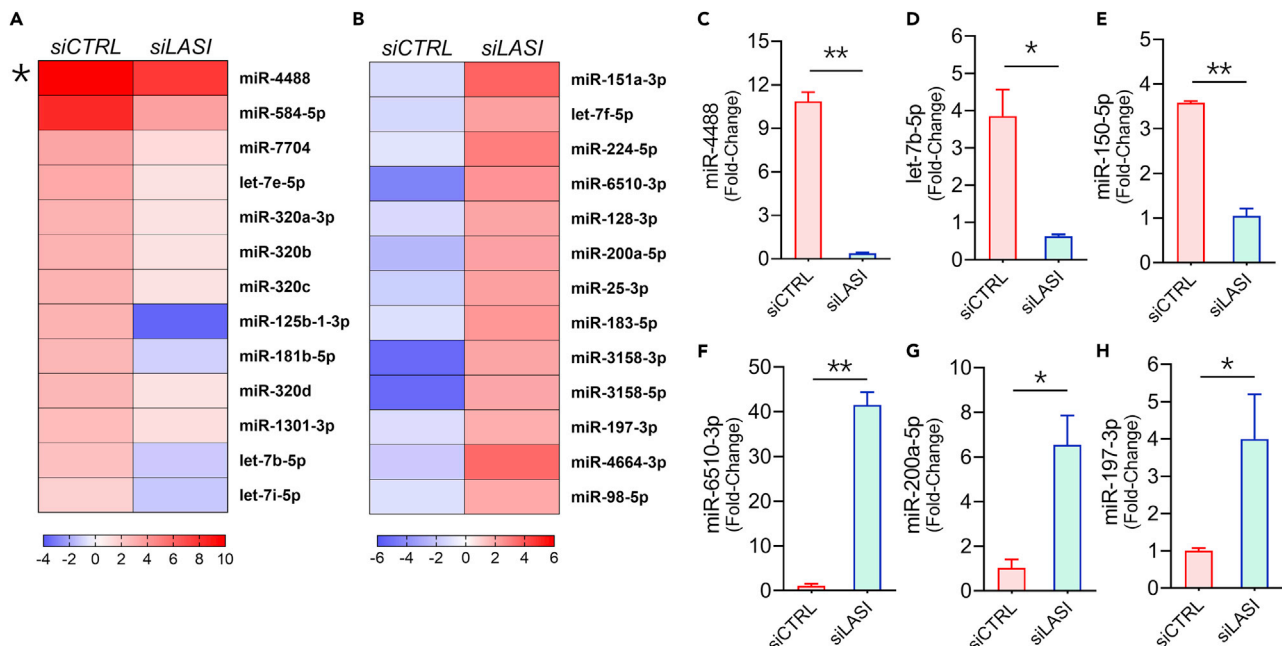
Figure 7. Airway epithelial miRNAs are modulated by SARS-CoV-2 infection and regulated by *LASI* lncRNA

Relative expression levels of miRNAs in si*LASI*-treated cells following 48 h SARS-CoV-2 infection compared with control-infected cells as analyzed by small RNA-seq analysis.

(A) Heatmap of select miRNAs upregulated by CoV-2 infection and suppressed in siLASI-treated cells (*miR-4488 was upregulated >200-fold in infected control cells); see Table S2 for the comprehensive list.

(B) Expression levels of miRNAs that are downregulated by CoV-2 infection but induced in si*LASI*-treated cells.

(C–E) Relative quantitation of miRNAs: (C) miR-4488, (D) let-7b-5p, and (E) miR-150-5p that were upregulated by SARS-CoV-2 infection in siCTRL cells but suppressed in siLASI-transfected cells.

(F–H) Relative expression of miRNAs: (F) miR-6510-3p, (G) miR-200a-5p, and (H) miR-197-3p that were downregulated by SARS-CoV-2 infection in siCTRL cells but induced in siLASI-transfected cells. (*p < 0.05; **p < 0.001 by Student's t test). Expression levels of select miRNAs were also elevated in Hi-VL nasopharyngeal swab samples of our study cohort (Figure S9).

important mediators of *LASI*-lncRNA-mediated modulation of CoV-2-induced airway epithelial mucoin-flammatory responses.

DISCUSSION

The pathogen-specific inflammatory response and subsequent successful resolution of inflammation and associated tissue remodeling in the upper respiratory tract determine the outcome of airborne infections. The SARS-CoV-2 infection continues to be a significant healthcare problem. Many studies suggest that dys-regulated inflammation and impaired ability to resolve inflammation and adjoining tissue remodeling are primary causes of increased morbidity and mortality among COVID-19 patients. Airway mucoinflammatory response, being the primary host defense system, is severely altered by SARS-CoV-2 infection. Not much is known about the immediate-early innate responses to SARS-CoV-2 infection. Thus, in this study, we focused on the effects of SARS-CoV-2 infection on airway mucus and inflammatory responses. We analyzed available RNA-seq data from COVID-19 patient nasal swab samples. We found that expressions of immunomodulatory lncRNAs, particularly *LASI* lncRNA, were altered in infected patients with elevated expression of mucoinflammatory factors. In our independent cohort of COVID-19 patients, the nasal SARS-CoV-2 viral load directly correlated with mucoinflammatory responses where COVID-19 patients with high Hi-VL showed elevated expression of mucins and inflammatory factors compared with Lo-VL pa-tients. Interestingly, we failed to detect any substantial changes in the expression of airway antiviral and interferon response genes in either cohort.

To understand the immediate-early response of AECs to SARS-CoV-2 infection, we examined a 3D human airway tissue model infected with high MOI of SARS-CoV-2 isolate USA-WI1/2020 (B.1.1.7). We observed elevated secretory mucins and inflammatory factors expression as early as 1 h postinfection. Among the

airway lncRNAs, we found *LASI* lncRNA expression strongly correlated with increased mucoinflammatory responses of the 3D airway tissue model.

Importantly, the roles of lncRNAs in the innate airway response to viral infection remain poorly understood. LncRNAs can interact with RNA, DNA/chromatin, and proteins and form RNA-RNA, RNA-DNA (RNA-chromatin), and RNA-protein complexes, leading to gene expression regulation via multiple mechanisms, including modulation of transcription, mRNA stability, and translation (Statello et al., 2021; Yao et al., 2019). Although little is known about specific lncRNA contributions to COVID-19 pathophysiology, several lncRNAs have now been suggested to potentially interact with SARS-CoV-2. Using the experimentally determined secondary structure of HOTAIR lncRNA (Somarowthu et al., 2015), a study recently predicted its interacting regions with spike RNA (Natarelli et al., 2021). LINC01505 has also been reported to bear a binding propensity for SARS-CoV-2 3′UTR. In addition, lncRNA H19 has been predicted to carry a significant binding potential for SARS-CoV-2 5′UTR and spike RNA (Natarelli et al., 2021). That said, logistic predictions suggest that most of these lncRNAs interactions, if true, would constitute negative modulators of CoV-2 infection.

In contrast, our data suggest that *LASI* lncRNA may be a positive modulator of CoV-2 infection. Our computational analyses identified a putative interaction between *LASI* lncRNA and SARS-CoV-2 Spike RNA, suggesting that *LASI* may act as a molecular scaffold or sponge for viral RNA, potentially protecting from degradation and/or other host factors. Regardless, we find inhibiting *LASI* lncRNA attenuates the SARS-CoV-2 viral load and alleviates the expression of inflammatory factors, mucins, and type-1 interferon (IFN) responsive genes in airway epithelial cells. Thus, targeting *LASI* may not only suppress the mucoinflammatory pathways but could also decrease the number of molecular scaffolds responsible for harboring the viral RNA and other components. Functional-RNA-based therapeutics are currently being actively pursued as potential treatment strategies due to minimal off-target effects to a high-efficiency presentation (Civenni, 2017), and lncRNA-targeted interventions can possibly mimic the mechanisms of many host immune response modulating RNAs (Winkle et al., 2021).

Acute inflammatory response to SARS-CoV-2 infection alters innate epithelial and vascular remodeling factors (Froberg and Diavatopoulos, 2021; Smith et al., 2021) with distinct inflammatory signatures reported among COVID-19 patients with low versus higher viral load (Cervia et al., 2021). Notably, the localized expression and secretion of ICAM-1 and IL-6 by respiratory epithelial cells may regulate airway responses and mucosal tissue remodeling (Manevski et al., 2020). In previous immunohistological analyses, IL-6 and ICAM-1 expression were reportedly higher in the alveolar epithelium of COVID-19 patients compared with H1N1-influenza-virus-infected patients or uninfected control subjects (Malaquias et al., 2021). We likewise find that ICAM-1 and IL-6 expressions are significantly higher in COVID-19 patients compared with controls, and patients with Hi-VL show increased expression of these inflammatory factors in our cohort.

Also of note, lncRNAs-mediated regulation of immune responses is potentially central to establishing airway mucosal immunity (Agirre et al., 2019; Devadoss et al., 2019; Ouyang et al., 2016) and could be dysregulated in COVID-19 patients. Numerous lncRNAs have been experimentally characterized and were shown to affect the immune responses of AEC, exert epigenetic changes, and induce the premature aging of the lung epithelium (Devadoss et al., 2019). However, among the lncRNAs analyzed, we found only *LASI* lncRNA expression to be consistently elevated in COVID-19 patients, although there were significant downregulations of *NEAT1* and *MALAT1* lncRNAs (Blanco-Melo et al., 2020), as recently confirmed in a separate computational analysis (Vishnubalaji et al., 2020). Further, we find that an acute effect of SARS-CoV-2 infection on airway mucin expression linked to *LASI* lncRNA expression could potentially hinder the effective mucociliary clearance of inhaled viral particles. We find the expressions of membrane-bound mucins were significantly upregulated during CoV-2 infection and that depleting *LASI* lncRNA could suppress the CoV-2-induced expression of these mucin genes. Airway mucins trap inhaled viral particles in the lumens and direct them toward the oropharynx via mucociliary clearance mechanisms. Any dysregulation of these processes leads to mucoinflammatory comorbidities and respiratory viral diseases (Holtzman et al., 2014; Ma et al., 2018). Excess mucus expression can lead to airway mucous obstruction due to mucin hyperexpression, hypersecretion, and goblet cell hyperplasia, and as reported here, SARS-CoV-2 alters these mucoinflammatory responses in agreement with other seminal studies (Desai et al., 2020; Lu et al., 2021; Smet et al., 2021; Yin et al., 2021). If not treated, these conditions can cause a decline in lung function and significantly higher morbidity and mortality. That said, our findings strongly suggest that *LASI* lncRNA constitutes an important master mucin regulator.

In addition, blocking *LASI* lncRNA expression in the 3D airway model led to a suppressed expression of MUC5AC protein levels following CoV-2 infection, implicating a direct role of *LASI* in viral-induced mucoinflammatory response. However, there was no change in any of the mucin regulating transcription factors' expression among CoV-2-infected cells, unlike our previous observation in the allergic asthma model (Devadoss et al., 2021a). This discrepancy observed between the effects of silencing LASI lncRNA in this and our previous study are unexpected and needs further investigation. Interestingly, among IFN response genes analyzed, blocking *LASI* expression suppressed the *IRF3* mRNA expression, with the expression of *IFNB1* mRNA also trending lower. In contrast, the upstream mediator *DDX58* mRNA expression was significantly induced in cells with suppressed *LASI* lncRNA levels and *IFIH1* mRNA trending toward a higher expression; this noted incongruity between type 1 IFN and its mediators needs more careful analysis, as it could potentially involve the RIG-1-like receptors engaged by siRNAs used for silencing *LASI* expression in our experimental set-up (Song and Rossi, 2017; van der Veen et al., 2018). Recent studies have also highlighted the differential role of DDX58 and IFIH1 in innate immune responses to CoV-2 infection and the role of the cellular lncRNAs therein (Brisse and Ly, 2019; Ji et al., 2022; Yang et al., 2021). However, the changes in IRF3 and DDX58 expression can also be a cause or consequence of lower infectivity in our experimental set-up as well as in the nasal samples analyzed.

There are various other small ncRNAs called miRNAs that interact with lncRNAs and modulate the gene expression and functions (Statello et al., 2021; Yao et al., 2019). We have also identified several putative miRNA candidates that could assist *LASI* lncRNA in modulating the mucoinflammatory response genes that contribute to airway inflammation and mucin expression. Our targeted small RNA-seq data implicated many host miRNAs that could possibly mediate the *LASI* lncRNA-based modulation of SARS-CoV-2 infection and associated inflammation. For example, following CoV-2 infection, a set of miRNAs including miR-4488, miR-584-5p, miR125-1-3p, miR-181b-5p, and let-7b-5p were highly upregulated but blocking the *LASI* lncRNA resulted in their downregulation compared with controls. These miRNAs might be facilitating the CoV-2 infection in a *LASI*-dependent manner, where *LASI* lncRNA may be acting as a molecular sponge or scaffold for these "inflammatory" miRNAs. There is very limited information about the role of these miRNAs. A computational prediction analysis performed by Pierce et al. identified that miR-181-5p binds to the mRNAs of both TMPRSS2 and IFN-γ in human lung tissue (Pierce et al., 2020). Another RNA-seq data analysis from SARS-CoV-2-infected lung tissues identified that miRNA let-7b-5p might be involved in COVID-19-associated lung pathologies (Chow and Salmena, 2020; Jafarinejad-Farsangi et al., 2020).

In contrast, specific miRNAs suppressed by CoV-2 infection were highly induced in siLASI-transfected cells, such as, miR-151a-3p, miR-6510-3p, miR-200a-5p, miR-25-3p, miR-3158-3p, miR-3158-5p, and miR-4644-3p. These miRNAs play an important role in regulating innate cellular responses and signaling pathways (Banaganapalli et al., 2021; Hosseini Rad Sm and McLellan, 2020), suggesting that these miRNAs are an important component of host immune response and are thus suppressed by CoV-2 infection in a mechanism dependent on *LASI* lncRNA levels. Based on the recent report on the interaction of miR-150-5p with CoV-2 nsp10 gene (Akula et al., 2022), we also found that CoV-2 infection modulates miR-150-5p expression in a *LASI*-dependent manner. It is noteworthy that nasal airway miR-150-5p expression was positively correlated with CoV-2 viral load in our cohort compared with the lower miR-150-5p levels reported in COVID-19 plasma samples (Akula et al., 2022). Further investigations are needed to determine the role of miR-150-5p in systemic versus pulmonary inflammation by examining the levels of cellular and plasma miR-150-5p collected from the same subjects. Thus, there is a large number of miRNAs that are directly impacted by *LASI* lncRNA and could be involved in CoV-2 infection and airway inflammatory response. We also found that there are a number of miRNAs whose expression was not significantly impacted by *LASI* lncRNA levels, such as miR-1301-3p, which is known to interact with CoV-2 genes/RNAs (Chow and Salmena, 2020; Sacar Demirci and Adan, 2020) and miR-320b, which interacts with viral NSP8 gene and is associated with transcription and replication of viral RNAs (Pierce et al., 2020).

Due to the combined colossal efforts of the continuous global surveillance and the large-scale vaccination drives, COVID-19 has been mitigated to a manageable endemic threat. Nonetheless, with a more significant proportion of the population still infected, the undetected and asymptomatic SARS-CoV-2 infections and invading vaccine/natural antibodies in vaccinated or infected individuals are resulting in the emergence of variants of concerns or VOCs (Kannan et al., 2021; Spratt et al., 2021), and thus, continuous efforts are needed to improve the current understanding on the host-pathogen interactions for these VOCs and to better prepare for any possible future viral outbreaks. The work presented here strongly suggests that

lncRNAs constitute a significant component of our innate immunity that directly interacts with viral RNA and describing these interactions may significantly improve our understanding of host factors involved in the viral response. Specifically, we report that *LASI* lncRNA in airway epithelial cells is not only a putative scaffold for SARS-CoV-2 RNA but also modulates respiratory mucoinflammatory responses. Thus, modulating specific functional lncRNA expression may aptly equip the host with innate immunity to combat the COVID-19 infection and associated mucoinflammatory comorbidities.

Limitations of the study

The nonavailability of a more significant number of patient nasal swab samples from COVID-19 subjects and the low yield of airway epithelial cells per sample may underscore the broader implications of the reported findings. The inadequate amount and quality of samples could have also contributed to the undiscernible and/or undetected levels of the genes analyzed that are expressed in low copy numbers such as genes regulating the antiviral and interferon response pathways. Further, our *in-vitro* studies primarily focused on the acute infection model, and we used high MOI of the original SARS-CoV-2 clinical isolate (B.1.1.7), and only the early time points were analyzed to understand the immediate-early changes in host innate response factors. The miRNAs identified to be responsible for *LASI* lncRNAs role in CoV-2 infection and associated inflammation need to be further validated by using the targeted molecular editing techniques as well as by longitudinally analyzing a larger study cohort.

STAR★METHODS

Detailed methods are provided in the online version of this paper and include the following:

- KEY RESOURCES TABLE
- RESOURCE AVAILABILITY
  - Lead contact
  - Materials availability
  - Data and code availability
- EXPERIMENTAL MODEL AND SUBJECT DETAILS
  - Datasets and bioinformatics
  - COVID-19 patient samples
  - Airway epithelial cell model of SARS-CoV-2 infection
- METHOD DETAILS
  - Immunostaining and fluorescent imaging analysis
  - Real-Time quantitative PCR for mRNAs, lncRNAs and miRNAs
  - Dual RNA fluorescent in-situ hybridization (FISH) and quantification
  - Enzyme-linked immunosorbent assays
  - Modeling of potential interaction site prediction and system preparation
  - System setup and molecular dynamics simulations
  - RNA interference-based lncRNA silencing
  - Small RNA sequencing analysis
- QUANTIFICATION AND STATISTICAL ANALYSIS

SUPPLEMENTAL INFORMATION

Supplemental information can be found online at https://doi.org/10.1016/j.isci.2022.104685.

AUTHOR CONTRIBUTIONS

DECLARATION OF INTERESTS

REFERENCES

Abdelmoaty, M.M., Yeapuri, P., Machhi, J., Olson, K.E., Shahjin, F., Kumar, V., Zhou, Y., Liang, J., Pandey, K., Acharya, A., et al. (2021). Defining the innate immune responses for SARS-CoV-2-human macrophage interactions. Front. Immunol. *12*, 741502. https://doi.org/10.3389/fimmu.2021.741502.

Acharya, A., Pandey, K., Thurman, M., Klug, E., Trivedi, J., Sharma, K., Lorson, C.L., Singh, K., and Byrareddy, S.N. (2021). Discovery and evaluation of entry inhibitors for SARS-CoV-2 and its emerging variants. J. Virol. *95*, e0143721. https://doi.org/10.1128/jvi.01437-21.

Abu-Izneid, T., AlHajri, N., Ibrahim, A.M., Javed, M.N., Salem, K.M., Pottoo, F.H., and Kamal, M.A. (2021). Micro-RNAs in the regulation of immune response against SARS CoV-2 and other viral infections. J. Adv. Res. *30*, 133–145. https://doi.org/10.1016/j.jare.2020.11.013.

Agirre, X., Meydan, C., Jiang, Y., Garate, L., Doane, A.S., Li, Z., Verma, A., Paiva, B., Martín-Subero, J.I., Elemento, O., et al. (2019). Long non-coding RNAs discriminate the stages and gene regulatory states of human humoral immune response. Nat. Commun. *10*, 821. https://doi.org/10.1038/s41467-019-08679-z.

Akula, S.M., Bolin, P., and Cook, P.P. (2022). Cellular miR-150-5p may have a crucial role to play in the biology of SARS-CoV-2 infection by regulating nsp10 gene. RNA Biol. *19*, 1–11. https://doi.org/10.1080/15476286.2021.2010959.

Antczak, M., Popenda, M., Zok, T., Sarzynska, J., Ratajczak, T., Tomczyk, K., Adamiak, R.W., and Szachniuk, M. (2016). New functionality of RNAComposer: an application to shape the axis of miR160 precursor structure. Acta Biochim. Pol. *63*, 737–744. https://doi.org/10.18388/abp.2016_1329.

Babicki, S., Arndt, D., Marcu, A., Liang, Y., Grant, J.R., Maciejewski, A., and Wishart, D.S. (2016). Heatmapper: web-enabled heat mapping for all. Nucleic Acids Res. *44*, W147–W153. https://doi.org/10.1093/nar/gkw419.

Banaganapalli, B., Al-Rayes, N., Awan, Z.A., Alsulaimany, F.A., Alamri, A.S., Elango, R., Malik, M.Z., and Shaik, N.A. (2021). Multilevel systems biology analysis of lung transcriptomics data identifies key miRNAs and potential miRNA target genes for SARS-CoV-2 infection. Comput. Biol. Med. *135*, 104570. https://doi.org/10.1016/j.compbiomed.2021.104570.

Baral, P., Bhattarai, N., Hossen, M.L., Stebliankin, V., Gerstman, B.S., Narasimhan, G., and Chapagain, P.P. (2021). Mutation-induced changes in the receptor-binding interface of the SARS-CoV-2 Delta variant B.1.617.2 and implications for immune evasion. Biochem. Biophys. Res. Commun. *574*, 14–19. https://doi.org/10.1016/j.bbrc.2021.08.036.

Blanco-Melo, D., Nilsson-Payant, B.E., Liu, W.C., Uhl, S., Hoagland, D., Møller, R., Jordan, T.X., Oishi, K., Panis, M., Sachs, D., et al. (2020). Imbalanced host response to SARS-CoV-2 drives development of COVID-19. Cell *181*, 1036–1045.e9. https://doi.org/10.1016/j.cell.2020.04.026.

Brisse, M., and Ly, H. (2019). Comparative structure and function analysis of the RIG-I-like receptors: RIG-I and MDA5. Front. Immunol. *10*, 1586. https://doi.org/10.3389/fimmu.2019.01586.

Camacho, C., Coulouris, G., Avagyan, V., Ma, N., Papadopoulos, J., Bealer, K., and Madden, T.L. (2009). BLAST+: architecture and applications. BMC Bioinf. *10*, 421. https://doi.org/10.1186/1471-2105-10-421.

Cervia, C., Nilsson, J., Zurbuchen, Y., Valaperti, A., Schreiner, J., Wolfensberger, A., Raeber, M.E., Adamo, S., Weigang, S., Emmenegger, M., et al. (2021). Systemic and mucosal antibody responses specific to SARS-CoV-2 during mild versus severe COVID-19. J. Allergy Clin. Immunol. *147*, 545–557.e9. https://doi.org/10.1016/j.jaci.2020.10.040.

Chand, H.S., Vazquez-Guillamet, R., Royer, C., Rudolph, K., Mishra, N., Singh, S.P., Hussain, S.S., Barrett, E., Callen, S., Byrareddy, S.N., et al.

(2018). Cigarette smoke and HIV synergistically affect lung pathology in cynomolgus macaques. J. Clin. Invest. *128*, 5428–5433. https://doi.org/10.1172/jci121935.

Cheemarla, N.R., Watkins, T.A., Mihaylova, V.T., Wang, B., Zhao, D., Wang, G., Landry, M.L., and Foxman, E.F. (2021). Dynamic innate immune response determines susceptibility to SARS-CoV-2 infection and early replication kinetics. J. Exp. Med. *218*, e20210583. https://doi.org/10.1084/jem.20210583.

Chen, G., Korfhagen, T.R., Karp, C.L., Impey, S., Xu, Y., Randell, S.H., Kitzmiller, J., Maeda, Y., Haitchi, H.M., Sridharan, A., et al. (2014). Foxa3 induces goblet cell metaplasia and inhibits innate antiviral immunity. Am. J. Respir. Crit. Care Med. *189*, 301–313. https://doi.org/10.1164/rccm.201306-1181oc.

Cheng, J., Zhou, X., Feng, W., Jia, M., Zhang, X., An, T., Luan, M., Pan, Y., Zhang, S., Zhou, Z., et al. (2021). Risk stratification by long non-coding RNAs profiling in COVID-19 patients. J. Cell Mol. Med. *25*, 4753–4764. https://doi.org/10.1111/jcmm.16444.

Chow, J.T.S., and Salmena, L. (2020). Prediction and analysis of SARS-CoV-2-targeting MicroRNA in human lung epithelium. Genes *11*, 1002. https://doi.org/10.3390/genes11091002.

Civenni, G. (2017). Targeting promoter-associated noncoding RNA in vivo. Methods Mol. Biol. *1543*, 259–270. https://doi.org/10.1007/978-1-4939-6716-2_15.

Cui, H., Banerjee, S., Guo, S., Xie, N., Ge, J., Jiang, D., Zörnig, M., Thannickal, V.J., and Liu, G. (2019). Long noncoding RNA Malat1 regulates differential activation of macrophages and response to lung injury. JCI Insight *4*, 124522. https://doi.org/10.1172/jci.insight.124522.

Desai, N., Neyaz, A., Szabolcs, A., Shih, A.R., Chen, J.H., Thapar, V., Nieman, L.T., Solovyov, A., Mehta, A., Lieb, D.J., et al. (2020). Temporal and spatial heterogeneity of host response to

SARS-CoV-2 pulmonary infection. Nat. Commun. 11, 6319. https://doi.org/10.1038/s41467-020-20139-7.

Devadoss, D., Long, C., Langley, R.J., Manevski, M., Nair, M., Campos, M.A., Borchert, G., Rahman, I., and Chand, H.S. (2019). Long noncoding transcriptome in chronic obstructive pulmonary disease. Am. J. Respir. Cell Mol. Biol. 61, 678–688. https://doi.org/10.1165/rcmb.2019-0184tr.

Devadoss, D., Daly, G., Manevski, M., Houserova, D., Hussain, S.S., Baumlin, N., Salathe, M., Borchert, G.M., Langley, R.J., and Chand, H.S. (2021a). A long noncoding RNA antisense to ICAM-1 is involved in allergic asthma associated hyperreactive response of airway epithelial cells. Mucosal Immunol. 14, 630–639. https://doi.org/10.1038/s41385-020-00352-9.

Devadoss, D., Singh, S.P., Acharya, A., Do, K.C., Periyasamy, P., Manevski, M., Mishra, N., Tellez, C.S., Ramakrishnan, S., Belinsky, S.A., et al. (2021b). HIV-1 productively infects and integrates in bronchial epithelial cells. Front. Cell. Infect. Microbiol. 10, 612360. https://doi.org/10.3389/fcimb.2020.612360.

Fageeh, H., Alshehri, A., Fageeh, H., Bizzoca, M.E., Lo Muzio, L., and Quadri, M.F. (2021). Re-infection of SARS-CoV-2: a case in a young dental healthcare worker. J. Infect. Public Health 14, 685–688. https://doi.org/10.1016/j.jiph.2021.02.012.

Fajnzylber, J., Regan, J., Coxen, K., Corry, H., Wong, C., Rosenthal, A., Worrall, D., Giguel, F., Piechocka-Trocha, A., Atyeo, C., et al. (2020). SARS-CoV-2 viral load is associated with increased disease severity and mortality. Nat. Commun. 11, 5493. https://doi.org/10.1038/s41467-020-19057-5.

Fliesser, E., Birnhuber, A., Marsh, L.M., Gschwandtner, E., Klepetko, W., Olschewski, H., and Kwapiszewska, G. (2021). Dysbalance of ACE2 levels - a possible cause for severe COVID-19 outcome in COPD. J. Pathol. Clin. Res. 7, 446–458.

Froberg, J., and Diavatopoulos, D.A. (2021). Mucosal immunity to severe acute respiratory syndrome coronavirus 2 infection. Curr. Opin. Infect. Dis. 34, 181–186. https://doi.org/10.1097/qco.0000000000000724.

Gruber, A.R., Bernhart, S.H., and Lorenz, R. (2015). The ViennaRNA web services. Methods Mol. Biol. 1269, 307–326. https://doi.org/10.1007/978-1-4939-2291-8_19.

He, X., Lau, E.H.Y., Wu, P., Deng, X., Wang, J., Hao, X., Lau, Y.C., Wong, J.Y., Guan, Y., Tan, X., et al. (2020). Temporal dynamics in viral shedding and transmissibility of COVID-19. Nat. Med. 26, 672–675. https://doi.org/10.1038/s41591-020-0869-5.

Hewitt, R.J., and Lloyd, C.M. (2021). Regulation of immune responses by the airway epithelial cell landscape. Nat. Rev. Immunol. 21, 347–362. https://doi.org/10.1038/s41577-020-00477-9.

Hoffmann, M., Kleine-Weber, H., Schroeder, S., Krüger, N., Herrler, T., Erichsen, S., Schiergens, T.S., Herrler, G., Wu, N.H., Nitsche, A., et al. (2020). SARS-CoV-2 cell entry depends on ACE2 and TMPRSS2 and is blocked by a clinically

proven protease inhibitor. Cell 181, 271–280.e8. https://doi.org/10.1016/j.cell.2020.02.052.

Holtzman, M.J., Byers, D.E., Brett, J.A., Patel, A.C., Agapov, E., Jin, X., and Wu, K. (2014). Linking acute infection to chronic lung disease. The role of IL-33-expressing epithelial progenitor cells. Ann. Am. Thorac. Soc. 11, S287–S291. https://doi.org/10.1513/annalsats.201402-056aw.

Hosseini Rad Sm, A., and McLellan, A.D. (2020). Implications of SARS-CoV-2 mutations for genomic RNA structure and host microRNA targeting. Int. J. Mol. Sci. 21, 4807. https://doi.org/10.3390/ijms21134807.

Hou, Y.J., Okuda, K., Edwards, C.E., Martinez, D.R., Asakura, T., Dinnon, K.H., 3rd, Kato, T., Lee, R.E., Yount, B.L., Mascenik, T.M., et al. (2020). SARS-CoV-2 reverse genetics reveals a variable infection gradient in the respiratory tract. Cell 182, 429–446.e14. https://doi.org/10.1016/j.cell.2020.05.042.

Humphrey, W., Dalke, A., and Schulten, K. (1996). VMD: visual molecular dynamics. J. Mol. Graph. 14, 33–38. https://doi.org/10.1016/0263-7855(96)00018-5.

Jafarinejad-Farsangi, S., Jazi, M.M., Rostamzadeh, F., and Hadizadeh, M. (2020). High affinity of host human microRNAs to SARS-CoV-2 genome: an in silico analysis. Noncoding RNA Res. 5, 222–231. https://doi.org/10.1016/j.ncrna.2020.11.005.

Ji, X., Meng, W., Liu, Z., and Mu, X. (2022). Emerging roles of lncRNAs regulating RNA-mediated type-I interferon signaling pathway. Front. Immunol. 13, 811122. https://doi.org/10.3389/fimmu.2022.811122.

Kannan, S.R., Spratt, A.N., Cohen, A.R., Naqvi, S.H., Chand, H.S., Quinn, T.P., Lorson, C.L., Byrareddy, S.N., and Singh, K. (2021). Evolutionary analysis of the delta and delta plus variants of the SARS-CoV-2 viruses. J. Autoimmun. 124, 102715. https://doi.org/10.1016/j.jaut.2021.102715.

Kannan, S.R., Spratt, A.N., Sharma, K., Chand, H.S., Byrareddy, S.N., and Singh, K. (2022). Omicron SARS-CoV-2 variant: unique features and their impact on pre-existing antibodies. J. Autoimmun. 126, 102779. https://doi.org/10.1016/j.jaut.2021.102779.

Lee, S., Kim, T., Lee, E., Lee, C., Kim, H., Rhee, H., Park, S.Y., Son, H.J., Yu, S., Park, J.W., et al. (2020). Clinical course and molecular viral shedding among asymptomatic and symptomatic patients with SARS-CoV-2 infection in a community treatment center in the Republic of Korea. JAMA Intern. Med. 180, 1447. https://doi.org/10.1001/jamainternmed.2020.3862.

Lee, J., Cheng, X., Swails, J.M., Yeom, M.S., Eastman, P.K., Lemkul, J.A., Wei, S., Buckner, J., Jeong, J.C., Qi, Y., et al. (2016). CHARMM-GUI input generator for NAMD, GROMACS, AMBER, OpenMM, and CHARMM/OpenMM simulations using the CHARMM36 additive force field. J. Chem. Theory Comput. 12, 405–413. https://doi.org/10.1021/acs.jctc.5b00935.

Li, G., Fan, Y., Lai, Y., Han, T., Li, Z., Zhou, P., Pan, P., Wang, W., Hu, D., Liu, X., et al. (2020). Coronavirus infections and immune responses.

J. Med. Virol. 92, 424–432. https://doi.org/10.1002/jmv.25685.

Lu, W., Liu, X., Wang, T., Liu, F., Zhu, A., Lin, Y., Luo, J., Ye, F., He, J., Zhao, J., et al. (2021). Elevated MUC1 and MUC5AC mucin protein levels in airway mucus of critical ill COVID-19 patients. J. Med. Virol. 93, 582–584. https://doi.org/10.1002/jmv.26406.

Ma, J., Rubin, B.K., and Voynow, J.A. (2018). Mucins, mucus, and goblet cells. Chest 154, 169–176. https://doi.org/10.1016/j.chest.2017.11.008.

Malaquias, M.A.S., Gadotti, A.C., Motta-Junior, J.D.S., Martins, A.P.C., Azevedo, M.L.V., Benevides, A.P.K., Cézar-Neto, P., Panini do Carmo, L.A., Zeni, R.C., Raboni, S.M., et al. (2021). The role of the lectin pathway of the complement system in SARS-CoV-2 lung injury. Transl. Res. 231, 55–63. https://doi.org/10.1016/j.trsl.2020.11.008.

Maltezou, H.C., Raftopoulos, V., Vorou, R., Papadima, K., Mellou, K., Spanakis, N., Kossyvakis, A., Gioula, G., Exindari, M., Froukala, E., et al. (2021). Association between upper respiratory tract viral load, comorbidities, disease severity, and outcome of patients with SARS-CoV-2 infection. J. Infect. Dis. 223, 1132–1138. https://doi.org/10.1093/infdis/jiaa804.

Manevski, M., Muthumalage, T., Devadoss, D., Sundar, I.K., Wang, Q., Singh, K.P., Unwalla, H.J., Chand, H.S., and Rahman, I. (2020). Cellular stress responses and dysfunctional Mitochondrial-cellular senescence, and therapeutics in chronic respiratory diseases. Redox Biol. 33, 101443. https://doi.org/10.1016/j.redox.2020.101443.

Mann, M., Wright, P.R., and Backofen, R. (2017). IntaRNA 2.0: enhanced and customizable prediction of RNA-RNA interactions. Nucleic Acids Res. 45, W435–W439. https://doi.org/10.1093/nar/gkx279.

Matusiak, M., and Schurch, C.M. (2020). Expression of SARS-CoV-2 entry receptors in the respiratory tract of healthy individuals, smokers and asthmatics. Respir. Res. 21, 252. https://doi.org/10.1186/s12931-020-01521-x.

Meydan, C., Madrer, N., and Soreq, H. (2020). The neat dance of COVID-19: NEAT1, DANCR, and Co-modulated cholinergic RNAs link to inflammation. Front. Immunol. 11, 590870. https://doi.org/10.3389/fimmu.2020.590870.

Morenikeji, O.B., Bernard, K., Strutton, E., Wallace, M., and Thomas, B.N. (2020). Evolutionarily conserved long non-coding RNA regulates gene expression in cytokine storm during COVID-19. Front. Bioeng. Biotechnol. 8, 582953. https://doi.org/10.3389/fbioe.2020.582953.

Mukherjee, S., Banerjee, B., Karasik, D., and Frenkel-Morgenstern, M. (2021). mRNA-lncRNA Co-expression network analysis reveals the role of lncRNAs in immune dysfunction during severe SARS-CoV-2 infection. Viruses 13, 402.

Natarelli, L., Parca, L., Mazza, T., Weber, C., Virgili, F., and Fratantonio, D. (2021). MicroRNAs and long non-coding RNAs as potential candidates to target specific motifs of SARS-CoV-2. Noncoding RNA 7, 14.

Olwenyi, O.A., Dyavar, S.R., Acharya, A., Podany, A.T., Fletcher, C.V., Ng, C.L., Reid, S.P., and Byrareddy, S.N. (2020). Immuno-epidemiology and pathophysiology of coronavirus disease 2019 (COVID-19). J. Mol. Med. (Berl.) 98, 1369–1383. https://doi.org/10.1007/s00109-020-01961-4.

Ouyang, J., Hu, J., and Chen, J.L. (2016). lncRNAs regulate the innate immune response to viral infection. Wiley Interdiscip. Rev. RNA 7, 129–143.

Phillips, J.C., Hardy, D.J., Maia, J.D.C., Stone, J.E., Ribeiro, J.V., Bernardi, R.C., Buch, R., Fiorin, G., Hénin, J., Jiang, W., et al. (2020). Scalable molecular dynamics on CPU and GPU architectures with NAMD. J. Chem. Phys. 153, 044130. https://doi.org/10.1063/5.0014475.

Pierce, J.B., Simion, V., Icli, B., Pérez-Cremades, D., Cheng, H.S., and Feinberg, M.W. (2020). Computational analysis of targeting SARS-CoV-2, viral entry proteins ACE2 and TMPRSS2, and interferon genes by host MicroRNAs. Genes 11, 1354. https://doi.org/10.3390/genes11111354.

Rajavelu, P., Chen, G., Xu, Y., Kitzmiller, J.A., Korfhagen, T.R., and Whitsett, J.A. (2015). Airway epithelial SPDEF integrates goblet cell differen- tiation and pulmonary Th2 inflammation. J. Clin. Invest. 125, 2021–2031. https://doi.org/10.1172/jci79422.

Ravindra, N.G., Alfajaro, M.M., Gasque, V., Huston, N.C., Wan, H., Szigeti-Buck, K., Yasumoto, Y., Greaney, A.M., Habet, V., Chow, R.D., et al. (2021). Single-cell longitudinal analysis of SARS-CoV-2 infection in human airway epithelium identifies target cells, alterations in gene expression, and cell state changes. PLoS Biol. 19, e3001143. https://doi.org/10.1371/journal.pbio.3001143.

Ridley, C., and Thornton, D.J. (2018). Mucins: the frontline defence of the lung. Biochem. Soc. Trans. 46, 1099–1106. https://doi.org/10.1042/bst20170402.

Rothan, H.A., and Byrareddy, S.N. (2020). The epidemiology and pathogenesis of coronavirus disease (COVID-19) outbreak. J. Autoimmun. 109, 102433. https://doi.org/10.1016/j.jaut.2020.102433.

Sacar Demirci, M.D., and Adan, A. (2020). Computational analysis of microRNA-mediated interactions in SARS-CoV-2 infection. PeerJ 8, e9369. https://doi.org/10.7717/peerj.9369.

Siniscalchi, C., Di Palo, A., Russo, A., and Potenza, N. (2021). Human MicroRNAs interacting with SARS-CoV-2 RNA sequences: computational

analysis and experimental target validation. Front. Genet. 12, 678994. https://doi.org/10.3389/fgene.2021.678994.

Smet, A., Breugelmans, T., Michiels, J., Lamote, K., Arras, W., De Man, J.G., Heyndrickx, L., Hauner, A., Huizing, M., Malhotra-Kumar, S., et al. (2021). A dynamic mucin mRNA signature associates with COVID-19 disease presentation and severity. JCI Insight 6, e151777. https://doi.org/10.1172/jci.insight.151777.

Smith, N., Goncalves, P., Charbit, B., Grzelak, L., Beretta, M., Planchais, C., Bruel, T., Rouilly, V., Bondet, V., Hadjadj, J., et al. (2021). Distinct systemic and mucosal immune responses during acute SARS-CoV-2 infection. Nat. Immunol. 22, 1428–1439. https://doi.org/10.1038/s41590-021-01028-7.

Somarowthu, S., Legiewicz, M., Chillón, I., Marcia, M., Liu, F., and Pyle, A. (2015). HOTAIR forms an intricate and modular secondary structure. Mol. Cell 58, 353–361. https://doi.org/10.1016/j.molcel.2015.03.006.

Song, M.S., and Rossi, J.J. (2017). Molecular mechanisms of Dicer: endonuclease and enzymatic activity. Biochem. J. 474, 1603–1618. https://doi.org/10.1042/bcj20160759.

Spratt, A.N., Kannan, S.R., Woods, L.T., Weisman, G.A., Quinn, T.P., Lorson, C.L., Sönnerborg, A., Byrareddy, S.N., and Singh, K. (2021). Evolution, correlation, structural impact and dynamics of emerging SARS-CoV-2 variants. Comput. Struct. Biotechnol. J. 19, 3799–3809. https://doi.org/10.1016/j.csbj.2021.06.037.

Statello, L., Guo, C.J., Chen, L.L., and Huarte, M. (2021). Gene regulation by long non-coding RNAs and its biological functions. Nat. Rev. Mol. Cell Biol. 22, 96–118. https://doi.org/10.1038/s41580-020-00315-9.

Turjya, R.R., Khan, M.A.A.K., and Mir Md Khademul Islam, A.B. (2020). Perversely expressed long noncoding RNAs can alter host response and viral proliferation in SARS-CoV-2 infection. Future Virol. 15, 577–593. https://doi.org/10.2217/fvl-2020-0188.

van der Veen, A.G., Maillard, P.V., Schmidt, J.M., Lee, S.A., Deddouche-Grass, S., Borg, A., Kjær, S., Snijders, A.P., and Reis e Sousa, C. (2018). The RIG-I-like receptor LGP2 inhibits Dicer- dependent processing of long double-stranded RNA and blocks RNA interference in mammalian cells. EMBO J. 37, e97479. https://doi.org/10.15252/embj.201797479.

Vishnubalaji, R., Shaath, H., and Alajez, N.M. (2020). Protein coding and long noncoding RNA (lncRNA) transcriptional landscape in SARS-CoV-2 infected bronchial epithelial cells highlight a role for interferon and inflammatory response. Genes 11, 760. https://doi.org/10.3390/genes11070760.

Vitale, J., Mumoli, N., Clerici, P., De Paschale, M., Evangelista, I., Cei, M., and Mazzone, A. (2021). Assessment of SARS-CoV-2 reinfection 1 Year after primary infection in a population in lombardy, Italy. JAMA Intern. Med. 181, 1407–1408. https://doi.org/10.1001/jamainternmed.2021.2959.

Weitnauer, M., Mijošek, V., and Dalpke, A.H. (2016). Control of local immunity by airway epithelial cells. Mucosal Immunol. 9, 287–298. https://doi.org/10.1038/mi.2015.126.

Winkle, M., El-Daly, S.M., Fabbri, M., and Calin, G.A. (2021). Noncoding RNA therapeutics - challenges and potential solutions. Nat. Rev. Drug Discov. 20, 629–651. https://doi.org/10.1038/s41573-021-00219-z.

Yang, D.M., Geng, T.T., Harrison, A.G., and Wang, P.H. (2021). Differential roles of RIG-I like receptors in SARS-CoV-2 infection. Mil. Med. Res. 8, 49. https://doi.org/10.1186/s40779-021-00340-5.

Yao, R.W., Wang, Y., and Chen, L.L. (2019). Cellular functions of long noncoding RNAs. Nat. Cell Biol. 21, 542–551. https://doi.org/10.1038/s41556-019-0311-8.

Yin, W., Cao, W., Zhou, G., Wang, L., Sun, J., Zhu, A., Wang, Z., Zhou, Y., Liu, X., Li, Y., et al. (2021). Analysis of pathological changes in the epithelium in COVID-19 patient airways. ERJ Open Res. 7. 00690-2020. https://doi.org/10.1183/23120541.00690-2020.

Yousefi, H., Poursheikhani, A., Bahmanpour, Z., Vatanmakanian, M., Taheri, M., Mashouri, L., and Alahari, S.K. (2020). SARS-CoV infection crosstalk with human host cell noncoding-RNA machinery: an in-silico approach. Biomed. Pharmacother. 130, 110548. https://doi.org/10.1016/j.biopha.2020.110548.

Zhang, X., Zhou, Y., Chen, S., Li, W., Chen, W., and Gu, W. (2019). LncRNA MACC1-AS1 sponges multiple miRNAs and RNA-binding protein PTBP1. Oncogenesis 8, 73. https://doi.org/10.1038/s41389-019-0182-7.

STAR★METHODS

KEY RESOURCES TABLE

REAGENT or RESOURCE	SOURCE	IDENTIFIER
Antibodies		
Anti-Mucin MUC5AC, clone CLH2 antibody	Millipore	Cat# MAB2011; RRID: AB_2146983
MUC5B antibody [19.4E]	Abcam	Cat# ab77995; RRID: AB_2146987
Donkey Anti-Mouse IgG (H+L) Antibody, Alexa Fluor 488 Conjugated	Invitrogen	Cat# A-21202; RRID: AB_141607
Bacterial and virus strains		
SARS-CoV-2 isolate USA-WI1/2020	BEI Resources	Cat# NR-52384
Biological samples		
Human Nasal Swabs	University of Miami	N/A
Human Nasal Swabs	iSpecimen	N/A
Chemicals, peptides, and recombinant proteins		
Tyramide Signal Amplification (TSA™) Plus Cyanine 5 System	PerkinElmer	Cat# NEL745001KT
Cyanin 3 Tyramine Signal Amplification (TSA) Fluorescence System Kit	APExBIO	Cat# K1051
MISSION® siRNA Transfection Reagent	Sigma-Aldrich	Cat#1452
TaqMan™ Universal PCR Master Mix	ThermoFisher	Cat# 4304437
iTaq Universal SYBR Green Supermix	BIORAD	Cat# 1725121
TaqMan™ Advanced miRNA cDNA Synthesis Kit	ThermoFisher	Cat# A28007
TaqMan™ Fast Advanced Master Mix	ThermoFisher	Cat# 4444557
DAPI Fluoromount-G®	SouthernBiotech	Cat# 0100-20
Collagen IV	Sigma-Aldrich	Cat# C5533
Critical commercial assays		
mucin-5AC (MUC5AC), ELISA Kit	MyBiosource	Cat#MBS701926
LEGEND MAX™ Human IL-6 ELISA Kit	BioLegend	Cat#430507
Human ICAM-1/CD54 (Sandwich ELISA) ELISA Kit	LifeSpan Biosciences	Cat# LS-F4019
RNAscope® Multiplex Fluorescent Detection Kit v2	Advanced Cell Diagnostics	Cat# 323110
RNAscope Probe-V-SARS-CoV-2-N-O1-C2	Advanced Cell Diagnostics	Cat# 863831-C2
RNAscope Probe-Hs-AC011511.2	Advanced Cell Diagnostics	N/A
iScript™ cDNA Synthesis Kit	BIORAD	Cat#1708891
RNeasy Mini Kit	Qiagen	Cat# 74106
Deposited data		
Sequence read archive (SRA) database	N/A	PRJNA730941
Experimental models: Cell lines		
Primary human airway epithelial cells	MATTEK	AIR-100
Primary human airway epithelial cells	Marsico Lung Institute Tissue Core, University of North Carolina	Normal HBE
Vero-STAT-1 knockout cells	ATCC	Cat# CCL-81-VHG; RRID:CVCL_YZ45

Continued

REAGENT or RESOURCE	SOURCE	IDENTIFIER
Experimental models: Organisms/strains		
A 3D mucociliary tissue model called EpiAirway that consists of normal, human-derived tracheal/bronchial epithelial cells were used in this study.	MatTek Corp	#AIR-100
Oligonucleotides		
SARS-CoV-2 nCoV_N1 Forward primer	Integrated DNA Technologies	Cat#10006821
SARS-CoV-2 nCoV_N1 Reverse primer	Integrated DNA Technologies	Cat#10006822
WAKMAR2 (AL35_X3 Set 1) PrimeTime® Std qPCR Assay	I Integrated DNA Technologies	Cat# 423484306
TaqMan gene expression assay-LASI	ThermoFisher	Cat# AR7DPYR
TaqMan gene expression assay-MALAT1	ThermoFisher	Cat# Hs00273907_s1
TaqMan gene expression assay-MUC5AC	ThermoFisher	Cat# Hs00873651_mH
TaqMan gene expression assay-MUC5B	ThermoFisher	Cat# Hs00861595_m1
TaqMan gene expression assay-SCGB1A1	ThermoFisher	Cat# Hs00171092_m1
TaqMan gene expression assay-FOXA3	ThermoFisher	Cat# Hs00270130_m1
TaqMan gene expression assay-GAPDH	ThermoFisher	Cat# Hs02786624_g1
PrimePCR™ SYBR® Green Assay-GAPDH	BIORAD	Cat# qHsaCED0038674
PrimePCR™ SYBR® Green Assay-MUC2	BIORAD	Cat# qHsaCID0011696
PrimePCR™ SYBR® Green Assay-MUC4	BIORAD	Cat# qHsaCID0021392
PrimePCR™ SYBR® Green Assay-MUC16	BIORAD	Cat# qHsaCID0018430
PrimePCR™ SYBR® Green Assay-MUC19	BIORAD	Cat# qHsaCID036986
PrimePCR™ SYBR® Green Assay-ICAM-1	BIORAD	Cat# qHsaCED0004281
PrimePCR™ SYBR® Green Assay-IL-6	BIORAD	Cat# qHsaCED0044677
PrimePCR™ SYBR® Green Assay-NEAT1	BIORAD	Cat# qHsaLED0134812
PrimePCR™ SYBR® Green Assay-SPDEF	BIORAD	Cat# qHsaCID0021209
PrimePCR™ SYBR® Green Assay-ACE2	BIORAD	Cat# qHsaCID0009100
PrimePCR™ SYBR® Green Assay-TMPRSS	BIORAD	Cat# qHsaCID0013558
PrimePCR™ SYBR® Green Assay-NRP1	BIORAD	Cat# qHsaCID0036359
PrimePCR™ SYBR® Green Assay-IFIH1	BIORAD	Cat# qHsaCID0006794
PrimePCR™ SYBR® Green Assay-DDX58	BIORAD	Cat# qHsaCED0043180
PrimePCR™ SYBR® Green Assay-IFNB1	BIORAD	Cat# qHSaCED0046851
PrimePCR™ SYBR® Green Assay-IRF3	BIORAD	Cat# qHsaCID0013112
TaqMan™ microRNA Control Assays- U6 snRNA	ThermoFisher	Cat# 001973
TaqMan™ Advanced miRNA Assay- hsa-miR-150-5p	ThermoFisher	Cat# 477918_mir
TaqMan™ Advanced miRNA Assay- hsa-let-7b-5p	ThermoFisher	Cat# 478576_mir
TaqMan™ Advanced miRNA Assay- hsa-miR-197-3p	ThermoFisher	Cat# 477959_mir
TaqMan™ Advanced miRNA Assay- hsa-miR-4488	ThermoFisher	Cat# 478906_mir
TaqMan™ Advanced miRNA Assay- hsa-miR-6510-3p	ThermoFisher	Cat# 480744_mir
TaqMan™ Advanced miRNA Assay- hsa-miR-125b-1-3p	ThermoFisher	Cat# 478665_mir

Continued

REAGENT or RESOURCE	SOURCE	IDENTIFIER
TaqMan™ Advanced miRNA Assay- hsa-miR-200a-5p	ThermoFisher	Cat# 478752_mir
MISSION® siRNA Fluorescent Universal Negative Control, Cyanine 3	Sigma-Aldrich	Cat# SIC003
Dicer-Substrate Short Interfering RNAs (DsiRNAs)-LASI:	Integrated DNA Technologies	N/A
Software and algorithms		
seqtk	N/A	https://github.com/lh3/seqtk
Ensembl Biomart		
BLAST+	NCBI	version 2.11.0
Image J	NIH	https://imagej.nih.gov/ij/download.html
IntaRNA 2.0 webserver	Mann et al., 2017	https://github.com/BackofenLab/IntaRNA/
RNAComposer	Antczak et al., 2016	https://rnacomposer.cs.put.poznan.pl/
RNAfold	Gruber et al., 2015	http://rna.tbi.univie.ac.at/cgi-bin/RNAWebSuite/RNAfold.cgi
CHARMM-GUI	Lee et al., 2016	http://www.charmm-gui.org
CUDA version of NAMD	Phillips et al., 2020	https://www.bio21.unimelb.edu.au/hpc/index.php/forums/cuda-version-of-namd
Charmm36m force field	Baral et al., 2021	https://www.charmm.org
visual molecular dynamics (VMD)	Humphrey et al., 1996	https://www.ks.uiuc.edu/Research/vmd/
GraphPad Prism v9.0	GraphPad	https://www.graphpad.com/
Heatmapper	Babicki et al., 2016	http://www.heatmapper.ca
Biorender	N/A	https://www.biorender.com/
Other		
BZX-700 Keyence All-in-One Microscope	Keyence Inc.	N/A

RESOURCE AVAILABILITY

Lead contact

Further information and requests for resources and reagents should be directed to and will be fulfilled by the lead contact, Hitendra S Chand.

Materials availability

This study did not generate new unique reagents.

Data and code availability

- Data reported in this paper will be shared by the lead contact upon request.

- This paper does not report original code.

- Any additional information required to reanalyze the data reported in this paper is available from the lead contact upon request

EXPERIMENTAL MODEL AND SUBJECT DETAILS

Datasets and bioinformatics

Raw RNA sequencing datasets were retrieved from the sequence read archive (SRA) database under accession no. PRJNA730941. Single-end FASTQ files for all COVID-19 patients and healthy controls (Table S1) were obtained using the SRA toolkit version 2.11.2 that was reported recently (Cheemarla et al., 2021). FASTQ files were converted to FASTA using seqtk (https://github.com/lh3/seqtk). Reads were aligned to a database consisting of select cDNA sequences (obtained from Ensembl Biomart) using BLAST+ (version 2.11.0). Alignments were required to uniquely map to a single cDNA and bear >94% identity

over 100 base pairs. Reads aligning to individual genes were enumerated and gene expression calculated in Reads Per Million (RPM).

COVID-19 patient samples

COVID-19 patient nasal swab samples (see Table 1 for demographics) were either obtained from the University of Miami Biobank facility or iSpecimen Inc. (Lexington, MA). There were 13 males and 7 females with the mean age of 62.5±3.51 y. Frozen cell pellets were processed for total RNA isolation and formalin-fixed cells were spread onto the slides for downstream analysis.

Airway epithelial cell model of SARS-CoV-2 infection

Studies involving SARS-CoV-2 virus infection were conducted at the University of Nebraska Medical Center BSL-3 high containment core facility. SARS-CoV-2 isolate USA-WI1/2020 (BEI; cat# NR-52384, B.1.1.7) was passaged in Vero-STAT-1 knockout cells and viral titer was determined using plaque assay (Abdelmoaty et al., 2021; Acharya et al., 2021). Primary human airway epithelial cells were purchased either from the Marsico Lung Institute Tissue Core (University of North Carolina) or from MatTek Incorp (EpiAirway™, MA). Airway epithelial cells were infected with 1 MOI of SARS-CoV-2 inoculum prepared in culture media. For 3D ALI cultured cells, 200 μL was added to the apical surface and 1 mL was added to the basal side. Infected transwells were incubated for 1 h at 37°C in 5% CO_2 incubator and the plates were gently mixed every 15 m. After 30 m, apical inoculum was removed and added to the basal media and after additional 30 m total virus inoculum was removed. Transwells were washed thoroughly with PBS and fresh media was added basally. Apical washes and basolateral medium culture supernatants were collected at 1, 4, 24, and 48 h post-infection (hpi) and stored at −80°C for downstream analysis, viral titration, and cytokine analysis. Cells were either lyzed in RLT buffer (RNeasy, Qiagen Inc) with 143 mM 2-ME for total RNA isolation or were fixed with 4% PFA (paraformaldehyde).

METHOD DETAILS

Immunostaining and fluorescent imaging analysis

Formalin-fixed cells were washed in 0.05% Brij-35 in PBS (pH 7.4) and immunostaining was performed as described previously (Chand et al., 2018). Cells were stained with antibodies to MUC5AC (Cat# MAB2011, Millipore Inc., Burlington, MA), and MUC5B (Cat# ab77995, Abcam, Boston, MA). Immunolabelled cells were detected using respective secondary antibodies conjugated fluorescent dyes (Jackson ImmunoResearch, PA) and images were captured using the BZX700 Microscopy system (Keyence Corp) and analyzed using NIH ImageJ software.

Real-Time quantitative PCR for mRNAs, lncRNAs and miRNAs

Total RNA was isolated from swabs or cells using the RNeasy kit (Qiagen, MD) as per the manufacturer's instructions. Primer/probe sets for *MUC5AC, MUC5B, SCGB1A1, FOXA3, LASI, WAKMAR2, NEAT1*, and *MALAT1* transcripts were obtained from Applied Biosystems (ThermoFisher Inc.), and the expression levels were quantified by qRT-PCR using TaqMan Gene expression kit (ThermoFisher Inc.). SYBR green-based primer sets for *SARS-CoV-2 N1 viral RNA, ACE2, TMPRSS2, NRP1, ICAM-1, IL-6, MUC2, MUC4, MUC16, MUC19, SPDEF, NEAT1, IFIH1, DDX58, IFNB1*, and *IRF3* mRNA were obtained from BioRad and quantified by qRT-PCR using the iTaq SYBR-green Master Mix (BioRad) in the BioRad CFX96 Real-Time PCR System. Relative quantities were calculated by normalizing data to GAPDH as described previously (Devadoss et al., 2021b). To detect the miRNA levels, cDNA was synthesized from isolated total RNA with a TaqMan® Advanced miRNA cDNA Synthesis Kit (Applied Biosystems, ThermoFisher Inc.). TaqMan® Advanced miRNA assays for *let-7b-5p, hsa-miR-150-5p, hsa-miR-197-3p, hsa-miR-200a-5p, hsa-miR-125b-1-3p* and *hsa-miR-4488* were obtained from Applied Biosystems (ThermoFisher Inc.), and the expression levels were quantified by qRT-PCR using TaqMan® Fast Advanced Master Mix (ThermoFisher Inc.). Relative quantities were calculated by normalizing data to *U6 snRNA* (Applied Biosystems, ThermoFisher Inc.).

Dual RNA fluorescent in-situ hybridization (FISH) and quantification

Dual-RNA FISH for LASI and SARS-CoV-2 N1 transcripts was performed using the RNAscope® Multiplex reagent kit (Advanced Cell Diagnostics, CA) per the manufacturer's protocol, the custom-made probe sets and as described recently (Devadoss et al., 2021b). Signals were amplified using Tyramide signal amplification (TSA) reaction using TSA-Plus Cy5 or Cy3 kit (PerkinElmer Bioscience) for *LASI* or SARS-CoV-2 N1 vRNA, respectively. Images were captured using a structured-illumination module of the

BZX700 Microscopy system and analyzed by NIH ImageJ software and RNA FISH expression was quantified as reported recently (Devadoss et al., 2021a). Briefly, RNA FISH expression was quantified by RNAscope® data analysis suite (Advanced Cell Diagnostics). Probe signals (dots)/cell were counted and allotted to separate bins as follows: Bin 0 (0 Dots/Cell); Bin 1 (1–3 Dots/Cell); Bin 2 (4–9 Dots/Cell); Bin 3 (10–15 Dots/Cell); Bin 4 (>15 Dots/Cell). Then, the Histo-score (H-Score) was calculated as follows: H-Score = Sum of each (bin number × percentage of cells per bin) i.e., H-score = (0 × % cells in Bin 0) + (1 × % cells in Bin 1) + (2 × % cells in Bin 2) + (3 × % cells in Bin 3) + (4 × % cells in Bin 4). Final scores derived by this metric have a range between 0 and 400.

Enzyme-linked immunosorbent assays

Apical washes and basal culture media supernatants from SARS-CoV-2 infected cells were analyzed for MUC5AC mucin and the inflammatory factors, interleukin-6 (IL-6) and intercellular adhesion molecule-1 (ICAM-1), protein levels. Apical washes were analyzed for MUC5AC mucin protein levels using specific ELISA (#MBS701926, MyBioSource Inc., CA) as per manufacturer's instructions. Levels of IL-6 (#430507, BioLegend Inc., CA) and soluble ICAM-1 (#LS-F4019, LifeSpan Biosciences Inc., WA) were measured in the basal culture media supernatants in separate ELISAs following manufacturers' instructions.

Modeling of potential interaction site prediction and system preparation

The IntaRNA 2.0 webserver (Mann et al., 2017) was used to predict potential RNA-RNA binding sites between the SARS-CoV-2 spike viral RNA and *LASI* lncRNA. The SARS-CoV-2 vRNA sequence 1227-1238 nucleotide (nt) was predicted to bind *LASI* lncRNA sequence at 635-646 nt. To generate a 3D structure of SARS-CoV-2 vRNA duplexed with the interacting sequence of *LASI* lncRNA, SARS-CoV-2 sequence from 1198-1268 nt was used. To allow *LASI* lncRNA nucleotides to base-pair with SARS-CoV-2 vRNA, we concatenated *LASI* lncRNA sequence 635-646 nt next to the SARS-CoV-2 vRNA 1227-1238. This tandem sequence was then used to predict the 3D structure using RNAComposer (Antczak et al., 2016) webserver, with the secondary structure information provided by RNAfold (Gruber et al., 2015). Finally, *LASI* lncRNA segment was renamed as a different chain (chain B), with remaining SARS-CoV-2 S vRNA sequence renumbered (chain A). Resulting complex is energy minimized, equilibrated, and further relaxed with molecular dynamics (MD) simulations.

System setup and molecular dynamics simulations

The CHARMM-GUI (Lee et al., 2016) Solution Builder tool was used to prepare the system for MD simulations. The solvated system with a physiological salt concentration of 0.15 M KCl contained a total of 87,000 atoms. All-atom MD simulations were performed using the CUDA version of NAMD 2.14 (Phillips et al., 2020) with the Charmm36m force field (Baral et al., 2021). Briefly, the structure was minimized for 10,000 steps with the steepest descent method and equilibrated for 125,000 steps with 2 fs timestep under NVT (constant volume and temperature) conditions. The production run was performed under NPT (constant pressure and temperature) conditions at a temperature of 303.15 K and a pressure of 1 bar. The production run consisted of 2 fs timesteps and a total of 50M steps collecting a 100-ns trajectory. Visualization and analysis of the trajectories were performed with visual molecular dynamics (VMD) (Humphrey et al., 1996).

RNA interference-based lncRNA silencing

The 3D cultured cells were transfected with siRNA specific to LASI (siLASI) or control siRNAs (siCTRL) using X2 (Mirus biotechnologies) transfection reagent (custom made by IDT technologies Inc.) as per manufacturer's instructions and as described recently (Devadoss et al., 2021a). After 48 h, cells were infected with 1 MOI of SARS-CoV-2 clinical isolate, and cells, apical wash and the basal media supernatant were analyzed at 48 hpi.

Small RNA sequencing analysis

Small RNA-seq was performed by Novogene inc. using an Illumina HiSeq v4 genome sequencer with 20M SE50 Reads. RNA was isolated from the 3D cultured airway cells infected with SARS-CoV-2 and transfected with siLASI to block LASI lncRNA expression. Briefly, Novogene employed the NEB-Next Multiplex Small RNA Library Prep Set for Illumina (NEB) coupled with automated agarose gel size selection (30 to 200 nt) using the Pipin Prep Instrument (Sage Science) for small RNA library preparation. Raw RNA sequencing datasets were retrieved, and FASTQ files were converted to FASTA using seqtk

(https://github.com/lh3/seqtk). Adapter sequences were removed with cutadapt, and reads were aligned to the GRCh38.P10 reference genome using BLAST+ (version 2.11.0) (Camacho et al., 2009). Alignments were required to uniquely map to a single position and bear 100% identity over at least 17 base pairs. Reads aligning to individual microRNAs were enumerated and gene expression calculated in Reads Per Million (RPM). Heat maps and unsupervised hierarchical clustering were generated using Heatmapper (Babicki et al., 2016).

QUANTIFICATION AND STATISTICAL ANALYSIS

Mean and standard error for replicates of the experiments were calculated, plotted, and analyzed using GraphPad Prism v9.0 (GraphPad Software Inc., San Diego, CA). Grouped results were analyzed using a one-way analysis of variance (ANOVA) with multiple comparisons, and student's t-test was used for data analysis between two groups. Data with FDR (false discovery rate) adjusted p-value threshold of ≤ 0.05 are considered as significantly relevant using Benjamini-Hochberg correction.